Meson exchange calculation of the $\bar{p}p \to \bar{\Lambda}\Lambda$ reaction

Frank Tabakin
University of Pittsburgh, Pittsburgh, Pennsylvania 15260

R. A. Eisenstein
Nuclear Physics Laboratory, University of Illinois, Champaign, Illinois 61820

(Received 23 January 1985)

The process $\bar{p}p \to \bar{\Lambda}\Lambda$ is studied using a one-boson t-channel strangeness exchange mechanism incorporating pseudoscalar, vector, and tensor mesons. Particular attention is paid to the spin degrees of freedom in the calculation. Initial and final state interactions, including the spin-orbit interaction and absorption, are taken into account using simple phenomenological models. The calculations are performed using density matrix ideas in the helicity basis, and the most important contributing amplitudes are identified. A reasonable fit to existing data can be obtained by allowing a smooth variation of the final state parameters with laboratory momentum. The effect of each of the exchanged mesons, and of the initial- and final-state baryon-baryon interactions on the cross sections and spin observables, is discussed. It is found that the tensor meson exchange plays an essential role even near threshold, which indicates the need for a detailed understanding of the short-range spin dynamics, perhaps as provided by future quark model studies.

I. INTRODUCTION

The low energy antiproton ring (LEAR) at CERN is now producing antiproton beams of unequaled intensity, beam purity, and momentum resolution.[1] High-precision experiments are thereby made possible, and should provide new knowledge about matter-antimatter interactions, and ultimately about the underlying quark dynamics. The mission of this facility may be characterized as a broad-scale study of the problems of low-energy quantum chromodynamics.

One of the experiments being performed[2] (PS-185) is an examination of hyperon-antihyperon ($\bar{Y}Y$) production following $\bar{p}p$ collisions. The problem is interesting because of its close similarity to interaction mechanisms in $\bar{p}p$ elastic scattering, but with the added requirement of strangeness exchange necessary to create the final state. Because the weak decay of the $\bar{Y}Y$ final state makes the process self-analyzing,[3] the final state polarizations and spin correlation coefficients can be measured without needing a second scattering. This determination, in addition to the differential and total cross sections, forms a nearly complete set of experimental measurements (at a given energy) for the process. Only the introduction of polarization into the initial state can constrain the process further.

In what follows, we discuss the process $\bar{p}p \to \bar{\Lambda}\Lambda$ as a sum of t-channel one-boson exchange diagrams, including the K (494, $J^\pi = 0^-$), the K* (890, $J^\pi = 1^-$) and the K** (1430, $J^\pi = 2^+$). [See Fig. 1(a).] Initial and final state absorption and spin-orbit interactions are included using simple eikonal ideas. Special emphasis is placed on the spin-dependent quantities, namely the polarizations of, and correlations between, the final state $\bar{\Lambda}$ and Λ spins. Our purpose is to provide a rather complete meson exchange calculation with which later quark-gluon model calculations can be compared. The simplest one-gluon exchange mechanism [Fig. 1(b)] is not likely to be able to describe the polarization data at either low or moderate energy; the reason for this is discussed in Sec. II E below. On the other hand, at the high momentum transfers required by this experiment even at threshold, the simple one-boson exchange picture is probably extended past its region of validity.

The first measurements[2] are a study of the $\bar{p}p \to \bar{\Lambda}\Lambda$ reaction near threshold, for which only a few partial waves are important in either the initial or final state. Also, the 0^-, 1^-, and 2^+ t-channel meson exchanges become quite simple at threshold, making the reaction observables easier to analyze phenomenologically. However, understanding the underlying quark dynamics will remain a difficult task, and our hope is to prepare for those studies by

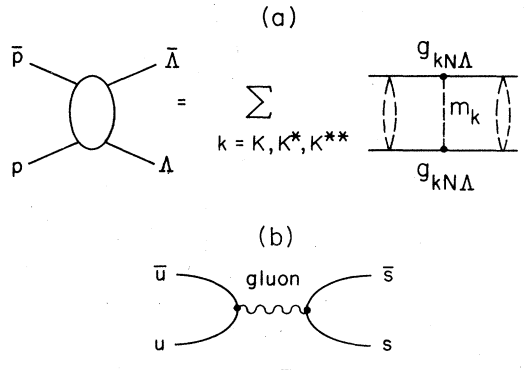

FIG. 1. (a) The process $\bar{p}p \to \bar{\Lambda}\Lambda$ viewed as a sum of single t-channel exchanges involving the K, K*, and K** mesons. The dashed ovals indicate initial- and final-state distortions using the method described in the text. (b) The simplest one-gluon exchange mechanism for converting the initial $\bar{u}u$ pair to the final $\bar{s}s$ pair.

first providing a determination of the role of short-range spin dynamics that the quark models must describe.

The calculations are formulated in the helicity basis[4,5] using a density matrix approach, from which all experimental observables can be easily obtained in any frame because the calculations are relativistically invariant. In addition, the effects of changes in the initial state beam and target polarizations can be easily studied. We have examined the sensitivity of the final polarizations and spin correlations to the various meson exchanges and have determined the role of each. Once the precision data are available, an important application of the methods developed here will be to extract the individual amplitudes directly from measurements.

Our work differs from earlier[6–15] peripheral model calculations by the inclusion of tensor meson exchange and by an improved treatment of the initial and final state interactions which includes an accounting for absorption and for a spin-orbit coupling. (For this purpose, we use the limited available experimental information of Refs. 16 and 17.) To the extent that these absorptive interactions are included, the Born approximation is relaxed. Previous work has shown that K (0^-) exchange alone does not suffice, as it yields backward-peaked differential cross sections. Thus K* (1^-) exchange must also be included. We extend the calculation by adding the K** (2^+) exchange as a probe of short distance behavior. If short-distance spin effects do play a role, then quark dynamics will probably have to be confronted. In addition, we include the effects of vertex form factors and the decay widths of the K* and K** mesons. We also compare our results to a very simple one-gluon exchange calculation, and show that the latter is unable to generate the necessary polarizations observed experimentally (at higher energies) in the final state.

The organization of the paper is as follows: Section II contains the details of the calculations leading from the initial $\bar{p}p$ state to the final four-particle $(\bar{p}\pi^+)(p\pi^-)$ state. Section III compares our results to previous work with the peripheral model and the Regge pole hypothesis;[18–22] Sec. IV gives our conclusions and suggested directions for future work. Two appendices are added as explanatory material.

II. DETAILS OF THE CALCULATION

A. General formulation

In this section we provide an outline of the calculation to be performed. To be able to include the effects of projectile and target spin, as well as to represent the intrinsic relativistic nature of the calculation, a density matrix formulation[4] is used in which the matrix elements are evaluated in the helicity basis.[4,5] The density matrix for the initial spin state is written as an outer product, whose separable form is valid since the beam and target are naturally prepared in an uncorrelated manner:

$$\rho_{\bar{p}p}=\tfrac{1}{4}(1+\boldsymbol{\sigma}\cdot\mathbf{P})_{\bar{p}}(1+\boldsymbol{\sigma}\cdot\mathbf{P})_{p} . \tag{1}$$

Here the $\boldsymbol{\sigma}$ are the Pauli spin matrices and the $\mathbf{P}$ are the initial polarizations of $\bar{p}$ and p.

The density matrix which describes the final state $(\bar{\Lambda}\Lambda$, for example) is obtained by operating on the initial state $\rho_{\bar{p}p}$ by the (angle-dependent) transition matrix T:

$$\rho_{\bar{\Lambda}\Lambda}=T(\theta)\rho_{\bar{p}p}T(\theta)^{\dagger} . \tag{2}$$

This matrix contains all experimentally available information about the $\bar{\Lambda}\Lambda$ system: We can, for example, obtain the differential cross section as

$$\frac{d\sigma}{d\Omega}=\frac{\mathrm{Tr}(\rho_{\bar{\Lambda}\Lambda})}{\mathrm{Tr}(\rho_{\bar{p}p})} , \tag{3}$$

or the density matrix for just one of the final state particles:

$$\rho_{\bar{\Lambda}}=\sum_{\Lambda}\rho_{\bar{\Lambda}\Lambda} . \tag{4}$$

The correlation between the spin components of the outgoing Λ particles [labeled (1) and (2)] is given by

$$C_{ij}=\mathrm{Tr}(\rho_{\bar{\Lambda}\Lambda}\sigma_i^{(1)}\sigma_j^{(2)})/\mathrm{Tr}(\rho_{\bar{\Lambda}\Lambda}) . \tag{5}$$

The experimental signature of the $\bar{p}p\rightarrow\bar{\Lambda}\Lambda$ process will be the weak decays of the $\bar{\Lambda}$ and the Λ, which yields a four-charged-particle state (see Fig. 2) via the processes $\Lambda\rightarrow p+\pi^-$ and $\bar{\Lambda}\rightarrow\bar{p}+\pi^+$. Because of charge conjugation symmetry these branches are equal and represent 64% of the total weak decays. Since the weak decay does not conserve parity, it is asymmetric with respect to the direction of the $\bar{\Lambda}$ (or Λ) polarization vector. This asymmetry is extremely useful experimentally, as it allows a determination of the final state polarizations without the need for a second scattering. The density matrix for the four-particle state is obtained by operating on $\rho_{\bar{\Lambda}\Lambda}$ with the weak decay T matrix T_w; viz.,

$$\rho_{\bar{p}\pi^+p\pi^-}=T_w\rho_{\bar{\Lambda}\Lambda}T_w^{\dagger} . \tag{6}$$

From this expression we may obtain the normalized angular distribution for the decay particles $\bar{p}$ and p moving along directions $\hat{\mathbf{k}}_{\bar{p}}$ and $\hat{\mathbf{k}}_{p}$ in their respective rest frames:

$$W(\hat{\mathbf{k}}_{\bar{p}},\hat{\mathbf{k}}_{p})=(16\pi^2)^{-1}\left[1+\bar{\alpha}\bar{P}_y\cos\bar{\theta}+\alpha P_y\cos\theta+\bar{\alpha}\alpha\sum_{ij}C_{ij}\cos\bar{\theta}_i\cos\theta_j\right] . \tag{7}$$

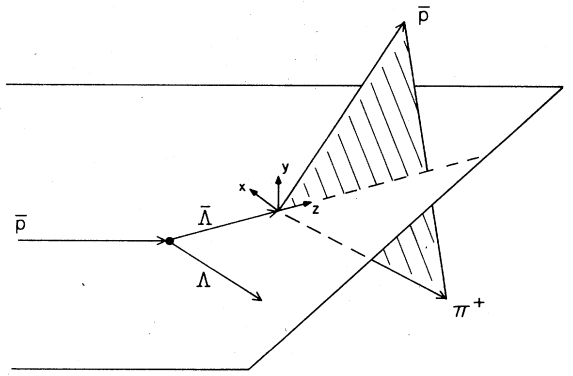

FIG. 2. Schematic laboratory view of the $\bar{p}p\rightarrow\bar{\Lambda}\Lambda$ reaction, followed by the weak decay $\bar{\Lambda}\rightarrow\bar{p}\pi^+$.

Here the indices (ij) stand for (x,y,z); $\bar{\alpha}$ and α are the weak decay asymmetry parameters, which are well known:[23] $\alpha = -\bar{\alpha} = 0.642 \pm 0.013$. All of the strong interaction physics of $\bar{p}p \to \bar{\Lambda}\Lambda$ is contained in the polarizations $\bar{P}_y$ and P_y, the correlation coefficients C_{ij}, and the total and differential cross sections. A more detailed derivation of the above form is given in Appendix A; the above result is obtained when there is no polarization in the initial state.

B. The strong interaction T-matrix $T(\theta)$

Calculation of the T matrix was carried out in the helicity formalism of Jacob and Wick;[5] the coordinate system used is shown in Fig. 3. In what follows, we make extensive use of the conventions established by Sopkovich.[6] Among the several advantages to be gained by using the helicity basis are the following: (1) because of relativistic invariance, the polarizations and correlation coefficients can easily be calculated in either the laboratory frame or in the individual rest frames; (2) the spin-dependent exchange diagrams are more easily evaluated than in an LS representation; and (3) the partial-wave expansion of the T matrix is very compactly expressed in terms of the Wigner $\mathscr{D}$ functions. The angle-dependent T matrix is written as (see Fig. 3)

$$\langle \mathbf{q}\bar{\lambda}'\lambda' \mid T(\theta,\phi) \mid \mathbf{p}\bar{\lambda}\lambda \rangle = \sum_J (2J+1)\langle J\bar{\lambda}'\lambda' \mid T \mid J\bar{\lambda}\lambda \rangle \mathscr{D}^{J*}_{\mu\mu'}(\phi,\theta,-\phi) , \tag{8}$$

where the $\mathscr{D}$ functions have labels corresponding to total angular momentum J and projections $\mu = \bar{\lambda} - \lambda$ and $\mu' = \bar{\lambda}' - \lambda'$. The helicities λ are the angular momenta of the particles projected along the directions $\mathbf{p}$ or $\mathbf{q}$. Depending on context in what follows, λ takes on values of $\pm\frac{1}{2}$ or ± 1. The quantities $\langle J\bar{\lambda}'\lambda' \mid T \mid J\bar{\lambda}\lambda \rangle$ are obtained from the strong interaction model used, and are described below.

The helicity basis states are not eigenstates of parity (see Appendix B). In order to write states of good parity, the following combinations of helicity states (for a given J) are formed:

$$\begin{aligned} |J1\rangle &= \frac{1}{\sqrt{2}}(|J+-\rangle - |J-+\rangle) , \\ |J3\rangle &= \frac{1}{\sqrt{2}}(|J++\rangle + |J--\rangle) , \\ |J2\rangle &= \frac{1}{\sqrt{2}}(|J+-\rangle + |J-+\rangle) , \\ |J4\rangle &= \frac{1}{\sqrt{2}}(|J++\rangle - |J--\rangle) . \end{aligned} \tag{9}$$

The notation used for the helicity states is $|J\bar{\lambda}\lambda\rangle$; the kets on the left make up the so-called number basis. Number states $|J1\rangle$ and $|J4\rangle$ are of parity $(-1)^{J+1}$, while $|J2\rangle$ and $|J3\rangle$ are of parity $(-1)^J$. (Recall that the intrinsic parity of an antifermion is -1.) The (unitary) transformation linking the helicity basis to the number basis is given by:

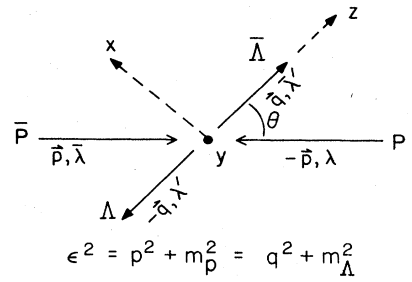

FIG. 3. The coordinate system used for the calculations presented in the text. The kinematic variables p and q are the initial and final state momenta in the center-of-momentum frame, while ϵ is the energy of any particle in that frame. The $\bar{\Lambda}$ is produced at an angle θ with respect to the incident $\bar{p}$ direction. The z axes are taken along the directions of the $\bar{p}$ and the $\bar{\Lambda}$, respectively, and the y axis is in the direction $\mathbf{p}\times\mathbf{q}$. The initial helicities are λ and $\bar{\lambda}$ for the p and $\bar{p}$, respectively; the final values are denoted by primes.

$$\langle J\bar{\lambda}\lambda \mid Jn \rangle = \frac{1}{\sqrt{2}} \begin{bmatrix} 1 & 1 & 0 & 0 \\ -1 & 1 & 0 & 0 \\ 0 & 0 & 1 & 1 \\ 0 & 0 & 1 & -1 \end{bmatrix} . \tag{10}$$

Here the rows have helicity labels $(+-)$, $(-+)$, $(++)$, and $(--)$; the columns are labeled 1, 2, 3, and 4. For self-conjugate final states, the number states are eigenstates of G parity [$G = C\exp(i\pi T_y)$]. State 1 has G parity $(-1)^{I+J+1}$, while states 2, 3, and 4 have G parity $(-1)^{I+J}$. For the $\bar{\Lambda}\Lambda$ final state, $I=0$. For the process $\bar{p}p \to \bar{\Lambda}\Lambda$, the restrictions due to conservation of parity and G parity lead to a transition matrix of the form:

$$\langle n' \mid T^{IJ} \mid n \rangle = \begin{bmatrix} A & 0 & 0 & 0 \\ 0 & B & D & 0 \\ 0 & F & C & 0 \\ 0 & 0 & 0 & E \end{bmatrix}^{IJ} . \tag{11}$$

Here A^{IJ} represents a transition between triplet states with $L=J$ and E^{IJ} a transition between singlet states. The other elements are transitions between triplet states with $L = J \pm 1$. Thus, six amplitudes are required to specify completely the transition for a given J and isospin I. For a non-self-conjugate final state (e.g., $\bar{p}p \to \bar{\Lambda}\Sigma$), which is not an eigenstate of G parity, eight amplitudes are required, giving

$$\langle n' \mid T^{IJ} \mid n \rangle = \begin{bmatrix} A & 0 & 0 & G \\ 0 & B & D & 0 \\ 0 & F & C & 0 \\ H & 0 & 0 & E \end{bmatrix}^{IJ} . \tag{12}$$

The L-S coupled states [$^3L_J (L = J$ and $L = J \pm 1)$ and ^1L_J] are simply related to the above number basis states by the following unitary transformation:

$$\begin{bmatrix}1\\2\\3\\4\end{bmatrix}_J = \begin{bmatrix} -1 & 0 & 0 & 0 \\ 0 & \left[\frac{J+1}{2J+1}\right]^{1/2} & \left[\frac{J}{2J+1}\right]^{1/2} & 0 \\ 0 & \left[\frac{J}{2J+1}\right]^{1/2} & -\left[\frac{J+1}{2J+1}\right]^{1/2} & 0 \\ 0 & 0 & 0 & 1 \end{bmatrix} \begin{bmatrix} {}^3L_J \\ {}^3L_J' \\ {}^3L_J'' \\ {}^1L_J \end{bmatrix} . \tag{13}$$

Here the notation is $L=J$, $L'=J-1$, and $L''=J+1$.

The states on the left-hand side have good parity, G parity, and total angular momentum J, but mixed helicity. The states on the right-hand side have good parity, G parity, total angular momentum J, and total spin S. In addition, their threshold behavior is simply understood because of the orbital angular momentum labels.

To proceed further, we take the incident $\bar{p}$ direction to define the z axis ($\theta=0$). Then, using Eq. (11) with transformation (10) in Eq. (8), and for convenience taking the azimuthal angle $\phi=0$, we find the helicity matrix elements to be

$$\langle \bar{\lambda}'\lambda' \mid T^I(\theta) \mid \bar{\lambda}\lambda \rangle = \frac{1}{2} \begin{bmatrix} 2A(\theta) & -2B(\theta) & -D(\theta) & -D(\theta) \\ -2B(\theta) & 2A(\theta) & D(\theta) & D(\theta) \\ F(\theta) & -F(\theta) & C(\theta)+E(\theta) & C(\theta)-E(\theta) \\ F(\theta) & -F(\theta) & C(\theta)-E(\theta) & C(\theta)+E(\theta) \end{bmatrix} . \tag{14}$$

In the process, six (independent) helicity amplitudes have been defined for a given isospin I:

$$\begin{aligned} A^I(\theta) &= \tfrac{1}{2}\sum_J (2J+1)(A^{IJ}+B^{IJ})d^J_{11}(\theta) = T^I(+-;+-) , \\ B^I(\theta) &= \tfrac{1}{2}\sum_J (2J+1)(A^{IJ}-B^{IJ})d^J_{1-1}(\theta) = -T^I(+-;-+) , \\ C^I(\theta) &= \sum_J (2J+1)C^{IJ}d^J_{00}(\theta) = \tfrac{1}{2}[T^I(++;++)+T^I(++;--)] , \\ D^I(\theta) &= \sum_J (2J+1)D^{IJ}d^J_{10}(\theta) = -T^I(+-;++) , \\ E^I(\theta) &= \sum_J (2J+1)E^{IJ}d^J_{00}(\theta) = \tfrac{1}{2}[T^I(++;++)-T^I(++;--)] , \\ F^I(\theta) &= \sum_J (2J+1)F^{IJ}d^J_{10}(\theta) = T^I(++;+-) . \end{aligned} \tag{15}$$

In these expressions the quantities $d^J_{\mu\mu'}(\theta)$ are the Wigner reduced d matrices,[27] and quantities T^I represent matrix elements: $T^I(+-;+-)=\langle +- \mid T^I(\theta) \mid +- \rangle$. The above amplitudes correspond to no helicity flip ($A, C+E$); single helicity flip (D, F); and double helicity flip ($B, C-E$).

Using Eqs. (2) and (3) we may now write the cross sections for $\bar{p}p \to \bar{\Lambda}\Lambda$ in terms of the isospin-0 amplitudes (where we now include a $\sqrt{2}$ factor from isospin and drop the $I=0$ label):

$$d\sigma/dt = (\pi/8p^2)(m_p m_\Lambda/\epsilon)^2(\mid A+B \mid^2 + \mid A-B \mid^2 + \mid C \mid^2 + \mid D \mid^2 + \mid E \mid^2 + \mid F \mid^2) , \tag{16}$$

$$\sigma(\bar{p}p \to \bar{\Lambda}\Lambda) = (\pi q/2p)(m_p m_\Lambda/\epsilon)^2 \sum_J (2J+1)(\mid A^J \mid^2 + \mid B^J \mid^2 + \mid C^J \mid^2 + \mid D^J \mid^2 + \mid E^J \mid^2 + \mid F^J \mid^2) . \tag{17}$$

In Eq. (16) the amplitudes appearing are the theta-dependent amplitudes of Eq. (15), while in Eq. (17) the amplitudes are the partial wave decomposed quantities. Kinematic variables are given in Fig. 3. Using the density matrix method, we may now calculate several important observables for the case when the beam and target are unpolarized:

$$\begin{aligned} P_y(\theta) &= 2\,\mathrm{Im}(A^*F+B^*F+C^*D)/I(\theta) , \\ \bar{P}_y(\theta) &= -P_y(\theta) , \\ C_{xx}(\theta) &= [\mid F \mid^2 + \mid C \mid^2 - \mid D \mid^2 - \mid E \mid^2 \\ &\quad -4\,\mathrm{Re}(A^*B)]/I(\theta) , \end{aligned} \tag{18, 19}$$

$$\begin{aligned} C_{yy}(\theta) &= [\mid F \mid^2 + \mid C \mid^2 + \mid D \mid^2 - \mid E \mid^2 \\ &\quad +4\,\mathrm{Re}(A^*B)]/I(\theta) , \end{aligned} \tag{20}$$

$$\begin{aligned} C_{zz}(\theta) &= [2(\mid A \mid^2 + \mid B \mid^2) + \mid D \mid^2 - \mid C \mid^2 \\ &\quad - \mid E \mid^2 - \mid F \mid^2]/I(\theta) , \end{aligned} \tag{21}$$

$$C_{zx}(\theta) = 2\,\mathrm{Re}(A^*F+B^*F+D^*C)/I(\theta) , \tag{22}$$

$$\begin{aligned} I(\theta) &= (\mid A+B \mid^2 + \mid A-B \mid^2 + \mid C \mid^2 + \mid D \mid^2 \\ &\quad + \mid E \mid^2 + \mid F \mid^2) . \end{aligned} \tag{23}$$

All of these quantities have been calculated using the Jacob-Wick conventions (Fig. 3). We note that the polarizations will be zero in the simple plane-wave one-boson-

exchange model. However, this will not be the case if the incoming and outgoing waves are distorted by complex potentials, or if the exchanged particle is allowed to have a complex mass to account for its decay.

Finally, we calculate the singlet fraction, which is the expectation value of the singlet projection operator $P_s=\frac{1}{4}(1-\boldsymbol{\sigma}_1\cdot\boldsymbol{\sigma}_2)$ and find $S_F=\frac{1}{4}(1-C_{xx}-C_{yy}-C_{zz})$, using the Jacob-Wick phase conventions. With the above expressions we obtain $S_F=|E|^2/I(\theta)$, as might be expected from the organization of the transition matrix in Eq. (11), from which it is apparent that E is the singlet amplitude. Triplet and coupled-state "fractions" could also be defined in this way.

We now proceed to a determination of the basic transition amplitudes, including initial and final state interactions, and use them to calculate the observables described above.

C. Calculation of exchange amplitudes

As mentioned earlier, we include in the t-channel exchange calculation the strangeness -1 mesons K, K*, and K**. The properties of these mesons, their propagators, and the vertex couplings used in the calculation, are given in Table I. Values of some of the coupling constants and guidance to the literature may be found in Ref. 24; further information was obtained from Rosenthal.[25] We note that there are phase changes associated with the antiparticle vertex couplings; these, and the phase of each state must be treated with great care (see Appendix B). What results is that the internal signs of each exchange term are determined by time reversal and parity, while the relative sign of each meson with respect to the others is determined by the Feynman rules and the Jacob and Wick phase conventions. (See Appendix B.) A point essential to our later discussion is the resulting *destructive interference* between the K* and K** meson exchanges. This situation is reminiscent of the discovery of the repulsive nature of vector meson exchange in the NN interaction.

In order to calculate the transition amplitude associated with each meson in the helicity basis, we first write the helicity spinors for particles (u) and antiparticles (v):

$$\begin{aligned}&\text{Particles: } u(\mathbf{p},\lambda)=N\begin{pmatrix}1\\ \lambda P\end{pmatrix}\mathscr{D}^{1/2}_{\lambda}(\hat{\mathbf{p}})\,,\\ &\text{Antiparticles: } v(\mathbf{p},\bar{\lambda})=N\begin{pmatrix}-\bar{\lambda}P\\ 1\end{pmatrix}\eta_{\lambda}\mathscr{D}^{1/2}_{-\bar{\lambda}}(\hat{\mathbf{p}})\,.\end{aligned}\tag{24}$$

Here $N=[(\epsilon+m)/2m]^{1/2}$, $P=p/(\epsilon+m)$, $\eta_\lambda=(-)^{1/2-\lambda/2}$, and the $\mathscr{D}^{1/2}_{\lambda}(\hat{\mathbf{p}})$ are, with $\phi=0$, for $\lambda=+1$ and -1, respectively,

$$\mathscr{D}^{1/2}_{1}(\hat{\mathbf{p}})=\begin{pmatrix}c\\ s\end{pmatrix},\quad \mathscr{D}^{1/2}_{-1}(\hat{\mathbf{p}})=\begin{pmatrix}-s\\ c\end{pmatrix}.$$

There are implicit spinor indices on the quantities u, v, and $\mathscr{D}$ in Eq. (24). These states have momentum $\mathbf{p}$ (along polar angle θ) and helicity label $\lambda=\pm1$. The quantities c and s are, respectively, $\cos(\theta/2)$ and $\sin(\theta/2)$. In what follows we use the conventions established by Bjorken and Drell[26] for the metric γ matrices and overall normalization ($\bar{u}u=1=-\bar{v}v$).

We now calculate the amplitude T_K for t-channel exchange of a pseudoscalar K$^-$ meson. It is of the form (see Figs. 1 and 3)

$$T_{\mathrm{K}}(\theta)=(g^2_{\mathrm{K}}/4\pi)(\bar{u}_{\lambda'}\gamma_5 u_{\lambda})(\bar{v}_{\bar{\lambda}}\gamma_5 v_{\bar{\lambda}'})(m^2_{\mathrm{K}}-t)^{-1}\,.\tag{25}$$

The product of vertex functions in the numerator is

$$\eta_{\bar{\lambda}}\eta_{\bar{\lambda}'}N^2_{\Lambda}N^2_{\mathrm{p}}(1,-\lambda' Q)\begin{bmatrix}0 & I\\ I & 0\end{bmatrix}\begin{bmatrix}1\\ -\lambda P\end{bmatrix}(-\bar{\lambda}P,-1)\begin{bmatrix}0 & I\\ I & 0\end{bmatrix}\begin{bmatrix}-\bar{\lambda}' Q\\ 1\end{bmatrix}M_u M_v\,,\tag{26}$$

with M_u and M_v given by

$$\begin{aligned}M_u&=\langle\lambda'|R(-\pi-\theta)R(\pi)|\lambda\rangle=d^{1/2}_{\lambda\lambda'}(\theta)\,,\\ M_v&=\langle-\bar{\lambda}|R(\theta)|-\bar{\lambda}'\rangle=d^{1/2}_{-\bar{\lambda}-\bar{\lambda}'}(\theta)\,.\end{aligned}\tag{27}$$

The product of these two d functions is proportional to $d^1_{\mu\mu'}(\theta)$ (see Ref. 27, p. 147). The quantity $Q=q/(\epsilon+m_\Lambda)$ and $N_\Lambda=[(\epsilon+m_\Lambda)/2m_\Lambda]^{1/2}$.

Equation (26) is then evaluated for each possible helicity combination. The results are used with Eq. (14) to obtain the amplitudes $A^I(\theta)$ to $E^I(\theta)$, which are given in Table II. We have here incorporated the phase convention of Jacob and Wick[4,5] for the helicity state of "particle 2"; in this case the incoming proton and outgoing lambda. (See Appendix B.)

TABLE I. Forms for the vertex couplings used in the present work. Here m_{p} is the proton mass; ϵ_μ and $\epsilon_{\mu\nu}$ are the spin functions for spin-one and spin-two particles. As described in Sec. III, the K** coupling was adjusted to give a good fit to the data. The other values are taken from Refs. 24 and 25. See the text.

Meson	Vertex coupling	Coupling constants $(g^2/4\pi)$
K (494)	$g_{\mathrm{K}}\gamma_5$	13.7
K* (892 + i50)	$g_{\mathrm{K}^*}\gamma_\mu\epsilon^{\mu *}$	8.77
K** (1430 + i100)	$\{(g_1/m_{\mathrm{p}})[(P_\Lambda+P_{\mathrm{p}})^\nu\gamma^\mu+(P_\Lambda+P_{\mathrm{p}})^\mu\gamma^\nu]$ $+(g_2/m^2_{\mathrm{p}})[(P_\Lambda+P_{\mathrm{p}})^\mu(P_\Lambda+P^\nu_{\mathrm{p}})]\}\epsilon^*_{\mu\nu}$	$g_1^2/4\pi=3.356$ $g_2^2/4\pi=0$

TABLE II. The amplitudes of Eq. (15). The terms multiplied by $h(\theta)$ are due to pseudoscalar K exchange; terms multiplied by $h^*(\theta)$ are due to vector K* exchange. The quantity $h(\theta)=\sqrt{2}(g_K^2/4\pi)N_pN_\Lambda(m_K^2-t)^{-1}$; $h^*(\theta)$ is the same expression evaluated for the K*. Here $c=\cos(\theta/2)$, $s=\sin(\theta/2)$, and all other symbols are defined in the text. Amplitudes B, C, E, and F incorporate the Jacob-Wick phase convention for "particle two."

$$A^I(\theta)=\{-(P-Q)^2h(\theta)-[R(PQ-1)^2+(P+Q)^2+(PQ+1)^2]h^*(\theta)\}c^2$$
$$B^I(\theta)=\{+(P+Q)^2h(\theta)+[R(PQ+1)^2+(P-Q)^2+(PQ-1)^2]h^*(\theta)\}s^2$$
$$C^I(\theta)=C_+^I(\theta)c^2+C_-^I(\theta)s^2$$
$$D^I(\theta)=\{-(P^2-Q^2)h(\theta)-[R(P^2Q^2-1)+(P^2Q^2-1)+(P^2-Q^2)]h^*(\theta)\}2cs$$
$$E^I(\theta)=E_+^I(\theta)c^2+E_-^I(\theta)s^2$$
$$F^I(\theta)=\{+(P^2-Q^2)h(\theta)-[R(P^2Q^2-1)+(P^2Q^2-1)-(P^2-Q^2)]h^*(\theta)\}2cs$$

$$C_+^I(\theta)=\{+(P-Q)^2h(\theta)-[R(1-PQ)^2+(P+Q)^2+(1+PQ)^2-2(P-Q)^2]h^*(\theta)\}$$
$$C_-^I(\theta)=\{-(P+Q)^2h(\theta)+[R(1+PQ)^2+(P-Q)^2+(1-PQ)^2-2(P+Q)^2]h^*(\theta)\}$$
$$E_+^I(\theta)=\{+(P-Q)^2h(\theta)-[R(1-PQ)^2+(P+Q)^2+(1+PQ)^2+2(P-Q)^2]h^*(\theta)\}$$
$$E_-^I(\theta)=\{+(P+Q)^2h(\theta)-[R(1+PQ)^2+(P-Q)^2+(1-PQ)^2+2(P+Q)^2]h^*(\theta)\}$$

The projections into partial waves of isospin I and angular momentum J to obtain the amplitudes for use in Eq. (15) can now be made. These partial wave decompositions are necessary if one wishes to insert appropriate damping in the low partial waves. This procedure, originally used by Sopkovich[6] and extended by others,[28–30] is discussed further in Sec. II E. Since the invariant momentum transfer $t=-p^2-q^2+2pq\cos\theta$, we may expand the propagator $(m_K^2-t)^{-1}$ in terms of Legendre functions of the first and second kind:[31]

$$[m_K^2-t]^{-1}=(2pq)^{-1}\sum_l(2l+1)P_l(\cos\theta)Q_l(z)\ , \qquad (28)$$

with $z=(p^2+q^2+m_K^2)/(2pq)$. Here p and q are the magnitudes of three-vectors. We then invert Eqs. (13) to obtain the partial wave amplitudes, using the relation[27]

$$d^A_{aa'}(\theta)d^B_{bb'}(\theta)=\sum_C(2C+1)\begin{bmatrix}A & B & C\\ a & b & c\end{bmatrix}\begin{bmatrix}A & B & C\\ a' & b' & c'\end{bmatrix}d^C_{cc'}(\theta)\ .$$

As an example, we obtain for A^{IJ} (including only pseudoscalar K exchange)

$$A^{IJ}=2(g_K^2/4\pi)N_\Lambda^2N_p^2(4pq)^{-1}\times\left[(a_J-b_J)+\frac{J}{2J+1}(a_{J+1}+b_{J+1})+\frac{J+1}{2J+1}(a_{J-1}+b_{J-1})\right]\ . \qquad (29)$$

Here $a_J=-(P-Q)^2Q_J(z)$ and $b_J=+(P+Q)^2Q_J(z)$. The other amplitudes are obtained in similar fashion.

Calculation of the exchange of the K* vector ($J^P=1^-$) meson is straightforward. The matrix element for vector coupling is written as

$$T_{K^*}(\theta)=-(g_{K^*}^2/4\pi)\sum_s(\bar u_{\lambda'}\gamma_\mu u_\lambda)(\bar v_{\bar\lambda}\gamma_\nu v_{\bar\lambda'})\times\epsilon^\mu(s)\epsilon^{\nu*}(s)\times(m_{K^*}^2-t)^{-1}\ , \qquad (30)$$

where we ignore the possibility of a magnetic coupling $\sigma_{\mu\nu}p^\nu\epsilon^\mu$. When the spin sums in the propagator are performed we find:

$$T_{K^*}(\theta)=-(g_{K^*}^2/4\pi)(m_{K^*}^2-t)^{-1}\times[R(\bar u_{\lambda'}u_\lambda)(\bar v_{\bar\lambda}v_{\bar\lambda'})-(\bar u_{\lambda'}\gamma_\mu u_\lambda)(\bar v_{\bar\lambda}\gamma^\mu v_{\bar\lambda'})]\ . \qquad (31)$$

Here $R=[(m_\Lambda-m_p)/m_{K^*}]^2$. We expand the propagator as in Eq. (28), allowing now the K* mass to be complex in order to account partly for the K* decay. The realization of Eq. (31) in the helicity basis leads to the expression

$$T_{K^*}(\theta)=(g_{K^*}^2/4\pi)\eta_{\bar\lambda}\eta_{\bar\lambda'}N_\Lambda^2N_p^2[-(\lambda P+\lambda'Q)(\bar\lambda P+\bar\lambda'Q)S(k,\lambda'\lambda)\bar S(k,-\bar\lambda-\bar\lambda')+(1+\lambda\lambda'QP)(1+\bar\lambda\bar\lambda'QP)d^{1/2}_{\lambda\lambda'}d^{1/2}_{-\bar\lambda-\bar\lambda'}](m_{K^*}^2-t)^{-1}\ . \qquad (32)$$

Here the functions $S(k)$ are given by $S(k)=\langle\lambda'\,|\,\sigma_k\,|\,\lambda\rangle$; the products $S(k)\bar S(k)$ are summed on k. These are given in Table III. As in the K case, both the product of the d functions and the sum over $S(k)\bar S(k)$ can be combined with the P_l function in the propagator to yield a single d function. In this way, Eq. (13) can again be used to identify the amplitudes. These are given in Table II.

We turn now to the evaluation of the t-channel K** ($J^P=2^+$) diagram. The appropriate vertex couplings are taken from Refs. 24 and 25; using the nomenclature in Fig. 3, we have

$$V^{\mu\nu}=\{(g_1/m_p\sqrt{4\pi})[(P_p+P_\Lambda)^\nu\gamma^\mu+(P_p+P_\Lambda)^\mu\gamma^\nu]+(g_2/m_p^2\sqrt{4\pi})(P_p+P_\Lambda)^\mu(P_p+P_\Lambda)^\nu\}\epsilon^*_{\mu\nu}(s)\ .$$

At the antiparticle vertex, the g_1 terms are multiplied by -1. The spin-two functions $\epsilon_{\mu\nu}(s)$ are constructed from the spin-one functions ϵ_μ as described by Refs. 32 and 33. The meson propagator will involve the following sum over polarizations:

$$P_{\mu\nu\mu'\nu'} = \sum_s \epsilon_{\mu\nu}(s)\epsilon^*_{\mu'\nu'}(s)$$
$$= \tfrac{1}{2}(P_{\mu\mu'}P_{\nu\nu'} + P_{\mu\nu'}P_{\nu\mu'}) - \tfrac{1}{3}P_{\mu\nu}P_{\mu'\nu'} , \quad (33)$$

with $P_{\mu\nu} = -g_{\mu\nu} + P_\mu P_\nu / m^2_{K^{**}}$. Here P_μ is the four-momentum carried by the exchanged meson, $m_{K^{**}}$ is the exchanged mass, and $g_{\mu\nu}$ is the metric tensor.[26] The resulting amplitude is

$$T_{K^{**}}(\theta) = -(g_1^2/4\pi m_p^2)(\bar{u}_{\lambda'} V^{\mu\nu} u_\lambda)(m^2_{K^{**}} - t)^{-1}$$
$$\times (\bar{v}_{\bar{\lambda}} V^{\mu'\nu'} v_{\bar{\lambda}'}) P_{\mu\nu\mu'\nu'} . \quad (34)$$

The evaluation of this amplitude is tedious, with result of the form

$$T_{K^{**}}(\theta) = -2(g_1^2/4\pi m_p^2) N_\Lambda^2 N_p^2 \eta_{\bar{\lambda}} \eta_{\bar{\lambda}'}$$
$$\times [D(x) f(x) + S(x) g(x)](m^2_{K^{**}} - t)^{-1} . \quad (35)$$

The quantity in square brackets depends on $x = \cos\theta$ and the initial and final state helicities. The functions $D(x)$ and $S(x)$ are the same products of d functions and products of $S(k)\bar{S}(k)$ given in Table III. For $f(x)$ and $g(x)$ we have

$$f(x) = f_0 + f_1 P_1(x) + f_2 P_2(x) ,$$
$$g(x) = g_0 + g_1 P_1(x) , \quad (36)$$

where the $P_l(x)$ are Legendre polynomials; the f_l and g_l quantities (which depend on helicity and kinematics) are given in Table IV. We note that in the equivalent expressions for the K and K*, f and g were independent of angle.

TABLE III. Helicity matrix of $\sum_k S(k,\lambda\lambda')\bar{S}(k,-\bar{\lambda}-\bar{\lambda}')$. The matrix for the d-function products is the same except for the lower right corner which is

$$\begin{bmatrix} c^2 & -s^2 \\ -s^2 & c^2 \end{bmatrix} .$$

In this table $c = \cos(\theta/2)$ and $s = \sin(\theta/2)$.

	$+-$	$-+$	$++$	$--$
$+-$	c^2	s^2	$-sc$	$-sc$
$-+$	s^2	c^2	sc	sc
$++$	sc	$-sc$	$-(1+s^2)$	$(1+c^2)$
$--$	sc	$-sc$	$(1+c^2)$	$-(1+s^2)$

We now expand the propagator as in Eq. (28), and combine the Legendre polynomials appearing there with those in Eq. (36). We obtain, using Ref. 25,

$$T_{K^{**}}(\theta) = -2[g_1^2/4\pi m_p^2 (2pq)] N_\Lambda^2 N_p^2 \bar{\lambda}\bar{\lambda}'$$
$$\times \left[D(x) \sum_c (2c+1)\alpha_c P_c(x) + S(x) \times \sum_c (2c+1)\beta_c P_c(x) \right] , \quad (37)$$

with

$$\alpha_l = f_0 \bar{Q}_{l0} + f_1 \bar{Q}_{l1} + f_2 \bar{Q}_{l2}$$

and

$$\beta_l = g_0 \bar{Q}_{l0} + g_1 \bar{Q}_{l1} .$$

We have for the $\bar{Q}$ functions:

TABLE IV. Algebraic quantities necessary for the evaluation of the K** (tensor) exchange amplitude. The momenta p and q are given in the text, as are the definitions of z, P, and Q.

$M = m_\Lambda + m_p$
$R = -g_2/g_1 m_p$
$\epsilon^2 = p^2 + m_p^2 = q^2 + m_\Lambda^2$
$a = 4\epsilon^2 + p^2 + q^2 + M^2\Delta^2$
$a' = 4\epsilon^2 - p^2 - q^2 - M^2\Delta^2$
$\alpha = \epsilon(aR - MX)$
$\beta = M^2X^2 + (1-XY)a + \frac{1}{2}a^2R^2 - \frac{1}{6}W^2$
$\Delta = (m_\Lambda - m_p)/m_K$
$X = 1 - \Delta^2$
$Y = 1 + 2MR$
$\delta = \frac{4}{3}p^2q^2$
$W = 2MX + a'R$
$\gamma = aR^2 + (1-XY) + \frac{1}{3}RW$

$A_0 = 16\epsilon^2 + a$
$A_1 = 8\alpha$
$A_2 = \beta + \frac{1}{3}\delta$
$A_3 = -a$

$B_0 = 2pq$
$B_1 = 16pq\epsilon R$
$B_2 = 2pq\gamma$
$B_3 = -2pq$
$C_2 = \frac{2}{3}\delta$

$H_0 = (1+\lambda\lambda'PQ)(1+\bar{\lambda}\bar{\lambda}'PQ)$
$H_1 = (1-\lambda\lambda'\bar{\lambda}\bar{\lambda}'P^2Q^2)$
$H_2 = (1-\lambda\lambda'PQ)(1-\bar{\lambda}\bar{\lambda}'PQ)$
$H_3 = (\lambda P + \lambda' Q)(\bar{\lambda}P + \bar{\lambda}'Q)$

$f_0 = A_0H_0 + A_1H_1 + A_2H_2$
$f_1 = B_0H_0 + B_1H_1 + B_2H_2$
$f_2 = C_2H_2$

$g_0 = A_3H_3$
$g_1 = B_3H_3$
$g_2 = 0$

$$\bar{Q}_{l0}=Q_l(z)\ ,$$

$$\bar{Q}_{l1}=\left[\frac{l}{2l+1}Q_{l-1}(z)+\frac{l+1}{2l+1}Q_{l+1}(z)\right]\ ,$$

$$\bar{Q}_{l2}=\left[\frac{3}{2}\frac{l(l-1)}{(2l-1)(2l+1)}Q_{l-2}(z)+\frac{l(l+1)}{(2l-1)(2l+3)}Q_l(z)+\frac{3}{2}\frac{(l+1)(l+2)}{(2l+3)(2l+1)}Q_{l+2}(z)\right]\ .$$

No Q_l functions with $l<0$ are allowed. The results for each of the six required amplitudes can now be obtained using Eq. (37) and Tables III and IV.

D. Checks on the calculation

In a calculation as detailed as this one, it is very useful to have available ways to check for algebraic errors and general physical consistency. We have principally used two such methods: one based on a parity argument, and one based on time reversal.

The time reversal check is based on the following: we note that in the nucleon-nucleon elastic scattering case, time reversal *invariance* requires that the amplitudes D and F of Eq. (12) be equal. (Thus, NN elastic scattering requires only five amplitudes.) In the case of $\bar{p}p\rightarrow\bar{\Lambda}\Lambda$, the time-reversed process is not equal to the original one, but is related to it by the reciprocity theorem. Thus, the amplitudes D and F can be checked using time reversal ideas in the following way: If we interchange the masses m_Λ and m_p, and the associated momenta q and p, then the amplitudes D and F are also interchanged. In this way each of these pieces of the meson exchanges can be checked via "time reversal reciprocity." Several errors in previous works were found in terms which were negligible at high energy but significant for our calculation.

The use of parity conservation provided another powerful check of our amplitudes, since two of the mesons exchanged are natural parity exchanges $(1^-,2^+)$, while the third has unnatural parity (0^-). Because of this, the total cross section calculated in Born approximation for unpolarized beam and target should show no interference between K and K* exchange or between K and K**. On the other hand, K* and K** do interfere with each other. The rule is proved (in Born approximation and spin averaged cases only) by noting that any interference terms between natural and unnatural parity exchanges will involve products of γ matrices, whose associated trace sums vanish for the natural-unnatural exchange interference terms. This rule proved very useful in checking our detailed amplitudes. When final/initial state interactions are included, however, interference effects will be generated.

Finally, we compared our results for the K and K* exchanges to those of other authors.[6–15] In cases of disagreement, our time-reversal and parity checks resolved the issue. Since our calculations pertain to the $\bar{\Lambda}\Lambda$ threshold region, we have not invoked several approximations suitable for higher energies that have been used in some other calculations.

E. Improvements on the Born approximation

In order to make a calculation with realistic predictive power, the Born approximation results of the previous sections must be modified. For example, the predicted polarizations of Eq. (18) will be zero in the model as it stands, because the strict Born approximation produces purely real amplitudes. The discussion so far has not yet taken into account the large absorption present in the incident $\bar{p}p$ channel, and has not dealt with the possibility of short-range cutoffs of the various meson-exchange diagrams. We also wish to examine the effects of the finite width for strong decay which is present in the K* and K** masses.

We begin with a discussion of the cutoff procedure used to eliminate the singular behavior of the meson exchange diagrams at short range. Such cutoffs have their origin in the dynamics occurring at the $p\Lambda K$ vertices, and ultimately are related to underlying quark wave functions. Such ideas suggest use of rather short-range exponential or Gaussian form factors; for simplicity we introduce multiple Yukawa forms.

In momentum space we invoke the cutoff by modifying the usual Yukawa propagator $1/(\mathbf{q}^2+m^2)$ for the exchanged particle of mass m by multiplying by the form factor $\Lambda_1^2/(\mathbf{q}^2+\Lambda_1^2)$. Thus

$$\frac{1}{\mathbf{q}^2+m^2}\frac{\Lambda_1^2}{\mathbf{q}^2+\Lambda_1^2}=\frac{\Lambda_1^2}{\Lambda_1^2-m^2}\left[\frac{1}{\mathbf{q}^2+m^2}-\frac{1}{\mathbf{q}^2+\Lambda_1^2}\right]\ . \tag{38}$$

The partial-wave decomposition of this expression will thus be modified, the $Q_l(z)$ of Eq. (28) being replaced by $\tilde{Q}_l(z)=F_1[Q_l(z)-Q_l(z_1)]$, with $F_1=\Lambda_1^2/(\Lambda_1^2-m^2)$ and $z_1=(p^2+q^2+\Lambda_1^2)/2pq$. The cutoff mass Λ_1 is taken to be $\Lambda_1=\zeta m$. For the 0^- meson a single cutoff is used. However, since the γ^μ coupling appears for the K*, we need at least two cutoffs for that meson. For the K** the $\gamma^\mu\partial_q$ coupling suggests using four multiplicative cutoffs. (The $\partial_\mu\partial_\nu$ term indicates use of six cutoffs for the g_2^{**} coupling.) To simulate even faster falloff, more multiplications can be included; a simple rule indicates how to proceed. For two and three cutoffs the expressions are

$$\tilde{Q}_l(z)=F_1F_2[Q_l(z)-G_{21}Q_l(z_1)-G_{12}Q_l(z_2)]$$

and

$$\tilde{Q}_l(z)=F_1F_2F_3[Q_l(z)-G_{21}G_{31}Q_l(z_1)-G_{12}G_{32}Q_l(z_2)-G_{23}G_{13}Q_l(z_3)]\ ,$$

with $G_{ij}=(\Lambda_i^2-m^2)/(\Lambda_i^2-\Lambda_j^2)$. Extension to other cases is straightforward. (Note that for $\Lambda\rightarrow\infty$ the above $\tilde{Q}_l$ functions return to the original irregular Legendre functions Q_l.) Use of these forms requires that the Λ values must each be distinct; for example, we have chosen for the four-cutoff case $\Lambda_1=\zeta m_{K^{**}}$, $\Lambda_2=\Lambda_1(1+\eta)$, and so on. To keep the number of parameters to a minimum, we have taken $\xi=5$ and $\eta=0.001$ in all cases. The effect of these cutoffs is discussed in Sec. III.

In order to study the effect of the finite widths for strong decay existing in the K* and K** cases, we have al-

lowed their masses to assume the complex values given in Table I. However, the Λ values for the cutoff masses were kept as real numbers. The effect of the finite widths is to make the argument z and hence the amplitudes slightly complex. Numerical results are given in Sec. III.

We turn now to our treatment of the initial and final state interactions. For the $\bar{p}p$ initial state, annihilation to multipion final states is a process that is about as large as elastic scattering and significantly larger than the charge exchange process. It is usual to account for this large depletion of flux in a phenomenological way, often by introducing absorptive potentials that are used in an optical model or coupled-channels approach. The existing elastic data[16,17] could be used to generate such a potential; however, such a detailed treatment may not be warranted at this stage due to the almost complete uncertainty regarding the final state interaction. We thus have opted to use, with appropriate extensions, a procedure originated by Sopkovich.[6]

In Sopkovich's theory, a model based in geometric optics is used to calculate the transition matrix element for each partial wave in a situation where the initial and final state, each described by an absorbing potential, are linked by a coupling potential given here by the meson exchanges. The development of these ideas[6] leads to this form for the modified T matrix:

$$\bar{T}^J_{fi}(\omega)=\sqrt{S^J_f(\omega)}\,T^J_{fi}(\omega)\sqrt{S^J_i(\omega)}\ . \tag{39}$$

Here T^J is the transition matrix from the Born approximation and the S^J are the matrices describing the initial and final state elastic scatterings. Due to the strong absorption in the initial state, it is clear that the T-matrix elements for the low partial waves will be the most strongly affected. We recognize that the derivation of Eq. (39) relies on high-energy eikonal ideas, while we are dealing at least for the final $\Lambda\bar{\Lambda}$ state with low (indeed threshold) energies. Nevertheless, the effects of the post and prior multipliers are to dampen waves. We could (and in the future shall) use proper initial and final state wave functions with associated integrations. In lieu of that, we simply use Eq. (39) and see what effect the damping of selected partial waves has on our set of observables.

In describing the incident channel we use the parametrization of Eisenhandler *et al.*,[16] which was obtained for $\bar{p}p$ elastic data taken over the range 690–2430 MeV/c. Their data are parametrized using the prescription of Daum *et al.*,[17] which is based on a strong absorption (Frahn-Venter) model containing a central and a spin-orbit piece: $V=V_c+V_{so}\mathbf{S}\cdot\mathbf{l}$. This model, due originally to Fermi, will give rise to significant polarization in the elastic scattering because of the absorption and surface-peaked spin-orbit term. Spin-spin effects are ignored and the scattering matrix is given by $M=f(\theta)+g(\theta)(\boldsymbol{\sigma}_1+\boldsymbol{\sigma}_1)\cdot\hat{\mathbf{n}}$, for which

$$f(\theta)=\frac{1}{k}\sum[(l+1)R^T_{l,l+1}+lR^T_{l,l-1}]P_l(x)$$

and

$$g(\theta)=\frac{i}{2k}\sum(R^T_{l,l+1}-R^T_{l,l-1})P^1_l(x)\ .$$

Here the R^T_{IJ} values are the partial-wave amplitudes for scattering in the triplet state, with $J=l\pm1$. These are related to the complex amplitudes $\eta_{l,J}$ via $R^T_{l,l\pm1}=(\eta^T_{l,l\pm1}-1)/2i$, with

$$\begin{aligned}&\mathrm{Re}\eta_{l,l\pm1}=h(t)+\epsilon[1-h(t)]\ ,\\ &\mathrm{Im}\eta_{l,l\pm1}=\mu_\pm\frac{dh(t)}{dt}\ .\end{aligned} \tag{40}$$

The expression for $h(t)$ is a continuous function of $t=l+\frac{1}{2}$ and is given by

$$h(t)=\{1+\exp[(kR-t)/kd]\}^{-1}\ .$$

We take R, d, and ϵ to be independent of l and J, as advocated by Daum *et al.*[17]

The connection between these amplitudes and the number-basis amplitudes in this paper are obtained from Eq. (2.24) of Bystricky *et al.* (Ref. 34) and our Eq. (13):

$$\begin{aligned}A^{IJ}&=\frac{1}{2J+1}[JR^T_{J,J+1}+(J+1)R^T_{J,J-1}]\\ &=R^T_{JJ}=R(^3L_{J=L})\ ,\\ B^{IJ}&=\frac{1}{2J+1}[JR^T_{J+1,J}+(J+1)R^T_{J-1,J}]\ ,\\ C^{IJ}&=\frac{1}{2J+1}[(J+1)R^T_{J+1,J}+JR^T_{J-1,J}]\ ,\\ D^{IJ}&=\frac{\sqrt{J(J+1)}}{2J+1}(R^T_{J-1,J}-R^T_{J+1,J})=F^{IJ}\ ,\\ E^{IJ}&=\frac{1}{2J+1}[(J+1)R^T_{J,J+1}+JR^T_{J,J-1}]\\ &=R(^1L_{J=L})\ .\end{aligned} \tag{41}$$

The model thus specifies the singlet ($^1L_{J=L}$) and triplet ($^3L_{J=L}$) amplitudes in terms of triplet $^3L_{J=L\pm1}$ amplitudes. Equations (40) are used to form the incident-channel S matrix needed for Eq. (39). Since the final state S matrices can be diagonalized by unitary matrices, the square root needed in Eq. (39) is readily constructed. Equation (40) reduces to the Sopkovich choice by simply taking R^T_{IJ} to be independent of l.

We turn now to a discussion of the final state. No data or theoretical predictions are available in the literature for the $\Lambda\bar{\Lambda}$ interaction near threshold; as a beginning ansatz we will make use of the above model, but with adjustable parameters R and d. We also vary the $\bar{\Lambda}\Lambda$ spin-orbit strengths $\mu_\pm$ using the $\bar{p}p$ case at the associated energies as a guide for our initial guesses. Our fits to the data are given below.

III. COMPARISON TO DATA

In order to investigate fully the effect of each of the meson exchanges included in our description of $\bar{p}p\to\bar{\Lambda}\Lambda$, we have used the data given in Refs. 35–38 to constrain our model. The data set used included some total cross section information[35] from near threshold to above 6 GeV/c incident $\bar{p}$ laboratory momentum (see Fig. 4) and also differential cross section information (Refs. 36–38)

at 1.85, 3.6, and 6.0 GeV/c.

In the calculations, the coupling constants for the K and K* were taken from Refs. 24 and 25, while the coupling for the K** was adjusted for best fit, as described below. The "global" value obtained is listed in Table I. For incident $\bar{p}$ laboratory momenta up to 2.2 GeV/c, the S-matrix elements obtained for elastic $\bar{p}p$ scattering obtained by Eisenhandler *et al.*[16] were taken over directly and used in Eq. (39) to distort the incoming $\bar{p}$ waves (see Table V). For our fits to the data at 3.6 and 6.0 GeV/c, other total cross section data[35] for $\bar{p}p$ were used to obtain parameters for use in the Eisenhandler ansatz. In all of the analysis, the final state $\bar{\Lambda}\Lambda$ S matrix (also using the Eisenhandler form) was adjusted, using a least squares search, to give a good fit to the data. The parameters obtained for these final states are given in Table V. The vertex form factors used are as described in Sec. II and were not adjusted; in addition, the real masses as given in Table I were used for the exchanged mesons. The sensitivity of our results to changes in the K* and K** cutoffs (Λ^* and Λ^{**}) prove to be quite significant. For example, at 6 GeV/c the differential cross section was quite insensitive to Λ^*, but halving Λ^{**} increased $\sigma(\theta)$ by a factor of 9, while doubling Λ^{**} decreased $\sigma(\theta)$ by about 40%. Since decreasing Λ^{**} cuts off higher momenta, the above behavior indicates a high sensitivity of $\sigma(\theta)$ to short-distance properties. On the other hand, the polarization and spin correlations proved to be quite insensitive to both Λ^* and Λ^{**}, which suggests that they are not sensitive to large q; perhaps because they are surface-dominated effects. Similar remarks hold for lower momenta. The use of the complex masses in Table I was an insignificant effect.

Figure 5 shows the resulting fits to the differential cross section data at 1.85, 3.6, and 6.0 GeV/c. The fits were obtained by making a global adjustment to the value of $g_{K^{**}}$ (i.e., the same value was used for all fits), followed by a case-by-case adjustment of the final state S-matrix parameters R, d, ϵ, and $\mu_\pm$ [see Eq. (39) and Table V]. We are encouraged by the fact that these values as a whole follow a smooth trend; it may or may not be significant that they do not differ substantially from the Eisenhandler values[16] for the $\bar{p}p$ incident channel. Having

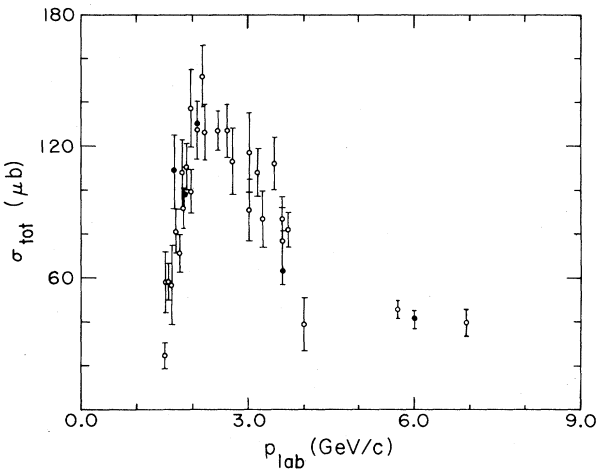

FIG. 4. The available total cross-section data for the process $\bar{p}p \rightarrow \bar{\Lambda}\Lambda$ (Ref. 35) plotted as a function of $\bar{p}$ laboratory momentum. The data used to obtain the final state "distortion" parameters for Eq. (40) are given by the heavy dots. See Table V. The data points at 3.6 and 6 GeV/c also required a fit to the incident $\bar{p}p$ channel, as the elastic data of Ref. 16 do not extend that high.

TABLE V. The parameters of Eq. (4) for the initial $\bar{p}p$ (denoted by I) and final $\bar{\Lambda}\Lambda$ (denoted by F) state interactions appropriate to the cases analyzed in this paper. The incident $\bar{p}$ laboratory momentum is given in the leftmost column, while the predicted total cross section is in the rightmost column.

$\bar{p}_{lab}$ (GeV/c)	Channel	R	d	μ_+	μ_-	ϵ	σ_{tot} (μb)
1.45	I	1.1187	0.1289	0.6631	−0.00337	0.03717	5.5
	F	4.6	0.117	0.95	1.08	0	
1.50	I	1.1074	0.1272	0.701	−0.0258	0.0531	24
	F	2.52	0.10	1.211	0.866	0	
1.65	I	1.0735	0.1220	0.8146	−0.0931	0.1009	109
	F	1.90	0.08	0.95	1.08	0	
1.85	I	1.06	0.1166	0.8395	−0.06946	0.1444	98
	F	1.624	0.079	0.95	1.08	0	
2.06	I	1.06	0.1115	0.8088	0.00634	0.1798	130
	F	1.5	0.075	0.95	1.08	0	
3.6	I	1.09	0.104	0.53	0.466	0.197	62
	F	1.858	0.131	1.0	0.92	0	
6.0	I	0.8	0.08	1.1	1.0	0	42
	F	1.91	0.15	1.211	0.866	0	

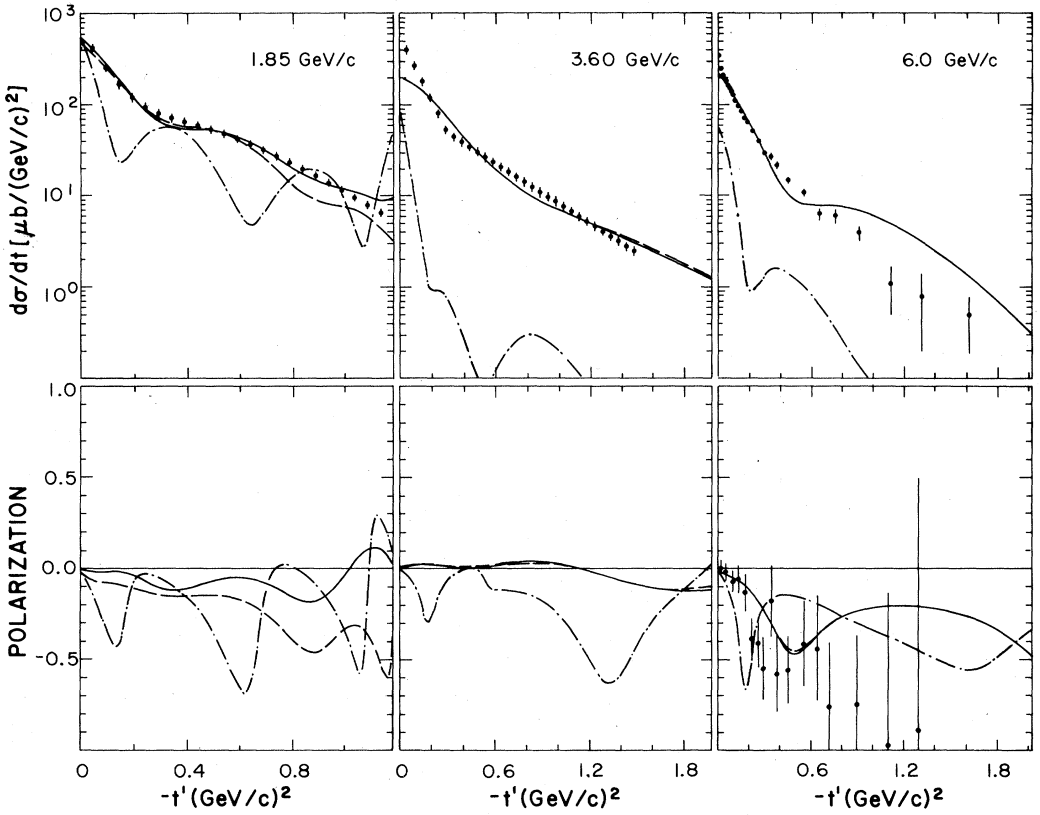

FIG. 5. Differential cross section and polarization data for the $\bar{p}p \to \bar{\Lambda}\Lambda$ processes at 1.85, 3.6, and 6.0 GeV/c incident $\bar{p}$ laboratory momenta, compared to our calculations. The data were obtained from Refs. 36—38, respectively. The 1.85 and 3.6 GeV/c sets shown here were obtained from functional forms given by the authors; we assigned a uniform 10% error bar to each point. The quantity t' along the abscissa is given by $t' = t - t_{\min}$. The solid curve in each plot represents our full calculation, including the K, K*, and K** mesons and the initial and final state distortions. The dashed curves result if the K meson is left out; the dash-dot curves are obtained if the K and K** are omitted. At 3.6 and 6.0 GeV/c the dashed curves are almost indistinguishable from the solid ones.

no guidance as to the size of the spin-orbit strength for the $\bar{\Lambda}\Lambda$ channel, our initial guesses for $\mu_\pm$ and ϵ were based on those for $\bar{p}p$ at the corresponding energy. As can be seen from Fig. 5, the resulting curves are in quite reasonable agreement with experiment. If the R and d values were allowed to depend on J, better fits would be possible.

Figure 5 also shows quite clearly the effect of each of the mesons exchanged. It has been known for some time (Refs. 6—15 and 18—22) that the effects of K (494) exchange are relatively unimportant compared to the K*; this is seen clearly in the figure, where it is apparent that the K (494) can be neglected at the higher energies. At the energies nearer the threshold, however, the K retains some importance for the differential cross section and especially for the polarization and spin correlation coefficients (Fig. 6). At the higher energies both the K* and K** play very important roles; in fact it is their *destructive interference* which allows a reasonable description of the data to be obtained. As described earlier, the relative phase is mandated by the quantum mechanics of the situation. (Without it, no reasonable value of the K** coupling constant or final-state interaction parameters could be found to bring the calculation even close to the data.) Indeed, the forward peaking shown in the data could not be duplicated without a suitable adjustment of the K** coupling constant. We also note that the present model does a reasonable job of describing the rather large measured polarization[38] at 6 GeV/c. Figures 5 and 6 also clearly show that the K** plays an important role even near the threshold. For this reason, we conclude that short-range interactions, and thus very likely the quark degrees of freedom, are an important part of the dynamics of this problem. We note in passing that even at threshold the momentum transfer involved in the process is quite substantial ($\sim 3F^{-1}$).

Figures 6 and 7 show the behavior of the spin correlation parameters C_{ij} as a function of incident $\bar{p}$ energy and as a function of the exchanged mesons. Very near threshold, where an s-wave interaction could be expected to dominate and the resulting amplitudes are very simple, the spin correlation coefficients are seen to be symmetric, or reflection symmetric, about 90°. As the energy increases, the curves depart from this simple behavior as more partial waves come into play. The interaction can also be modified by altering the basic meson exchanges;

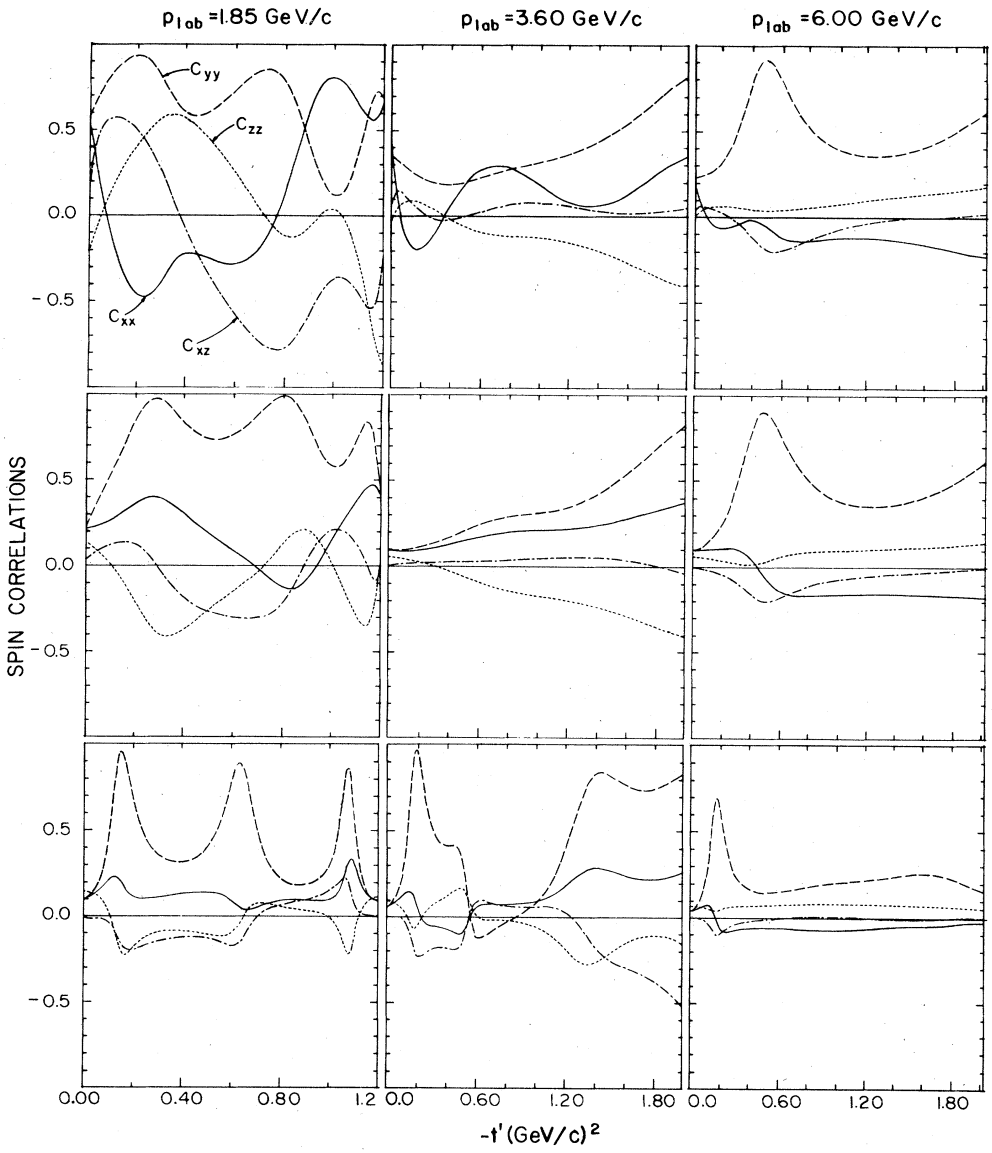

FIG. 6. Predictions for the spin correlation coefficients at 1.85, 3.6, and 6.0 GeV/c. The top row contains the results of the full calculation, the middle row has the results leaving out the K meson, and the bottom row has the result of leaving out the K and K** mesons. See also Fig. 5.

this is shown in the middle and bottom panels of Fig. 6. As the various mesons are turned on and off the C_{ij} are changed radically in both shape and sign. It is somewhat surprising that the K meson plays as important a role as it seems to. It is clear that these coefficients (and the polarization) are extremely sensitive to the dynamical content of the reaction mechanism.

The purpose of Fig. 7 is to show that in the energy region where the recent LEAR experiments have been done (1.480 and 1.507 GeV/c laboratory $\bar{p}$ momentum), the polarization and the spin correlations are sizable. While it is true that as the threshold for the reaction is approached the polarization must vanish, the spin correlations need not. (It is because of parity conservation[3] that the correlation coefficients $C_{xy}=C_{yx}=C_{yz}=C_{zy}=0$.)

Figure 8 shows the behavior with energy of the amplitudes given by Eq. (15). At low energies all of the amplitudes are significantly different from each other, and all are important, although in different regions of t. The non-helicity-flip amplitudes $(A,C+E)$ are moderately forward peaked. As the energy increases, the picture simplifies considerably; the amplitudes corresponding to double helicity flip $(B,C-E)$ are greatly diminished, while the single-flip amplitudes (D,F) remain of moderate size, and the non-helicity-flip amplitudes $(A,C+E)$ are very large in the forward direction. This behavior has been observed previously in Regge pole treatments[18–22] of this reaction; however, as our analysis shows, it would be wrong to extend their conclusions (which are after all based on a high-energy model) to the threshold regime.

Figure 9 shows the contributions of each meson to the partial-wave projected amplitudes of Eq. (15). To make

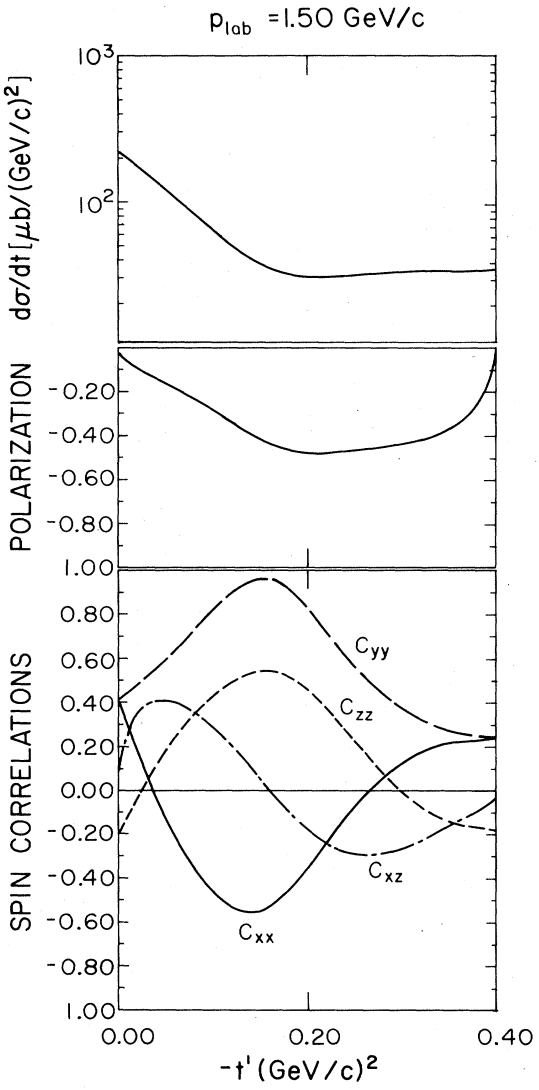

FIG. 7. Predictions of the full calculation for the differential cross section, the polarization, and the spin correlation coefficients at 1.50 GeV/c, just above the reaction threshold at 1.435 GeV/c laboratory momentum. See also Fig. 5.

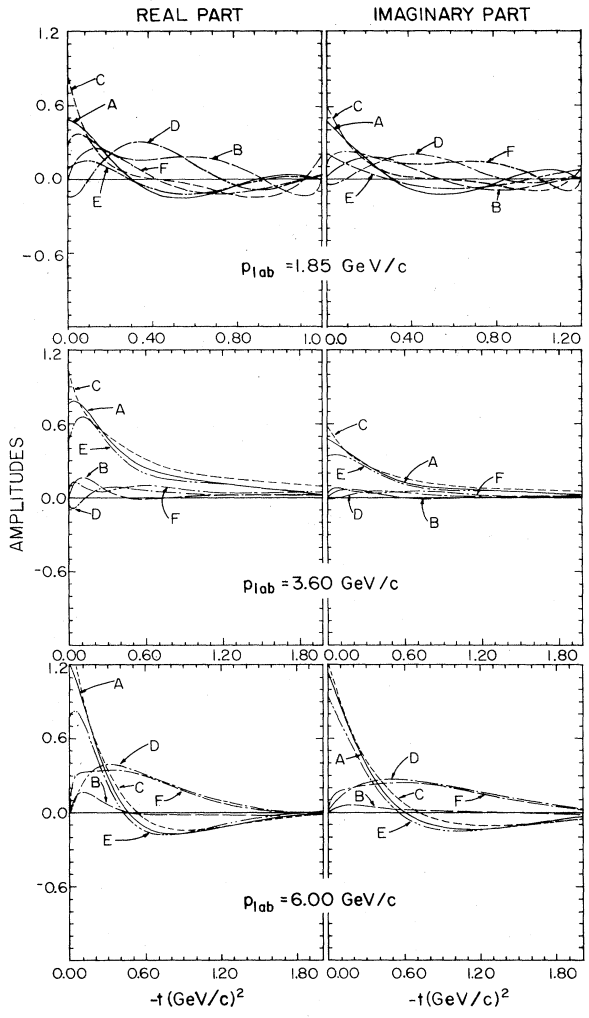

FIG. 8. The real and imaginary parts of the amplitudes of Eq. (15), shown here as a function of invariant momentum transfer squared, for incident p momentum of 1.85, 3.6, and 6.0 GeV/c. Amplitudes A and $C+E$ represent no helicity flip, D and F are single helicity flip, while B and $C-E$ correspond to double helicity flip. See also Fig. 5.

more explicit contact with other models of strong nuclear forces, these amplitudes are given in the L-S basis. We see that in the case of the K meson the strength ordering of the amplitudes follows that of a tensor force; this is to be expected because the structure of the (pseudoscalar) one-kaon exchange potential (OKEP) is identical to the one-pion exchange potential (OPEP) model. On the other hand, the exchange of K* and K** mesons, with their vector and tensor characters, gives rise to potential structures with strong $L\cdot S$ components. This is observed in Fig. 9 in the ordering of the strengths of their amplitudes, which follow that of an $L\cdot S$ force.

As we have indicated earlier, the role of initial and final state interactions in this problem is an extremely important one. This is true for at least two reasons: (1) the strong absorption present in both the initial and final state makes the strict Born approximation useless for obtaining the proper magnitude for the cross sections; and (2) within the model used here the only way to generate sizable polarization is through absorptive entrance- and exit-channel spin-orbit forces. (The use of complex masses to simulate the decay of the exchanged K* and K** mesons has only a very minor effect on either of these questions.) Thus, while the magnitude of the polarization induced by the initial and final state can be strongly modified by the nature of the meson exchange mechanism, it would be identically zero in our model without the initial and final state interactions and the small effect of the complex exchanged meson mass. This is not true of the spin-correlations C_{ij}, as they *do not* require any initial or final state interaction to generate them. They can also be sizable at threshold, where the polarization vanishes.

The effect on the cross section magnitudes is equally dramatic. Figure 10 shows the result of turning off the

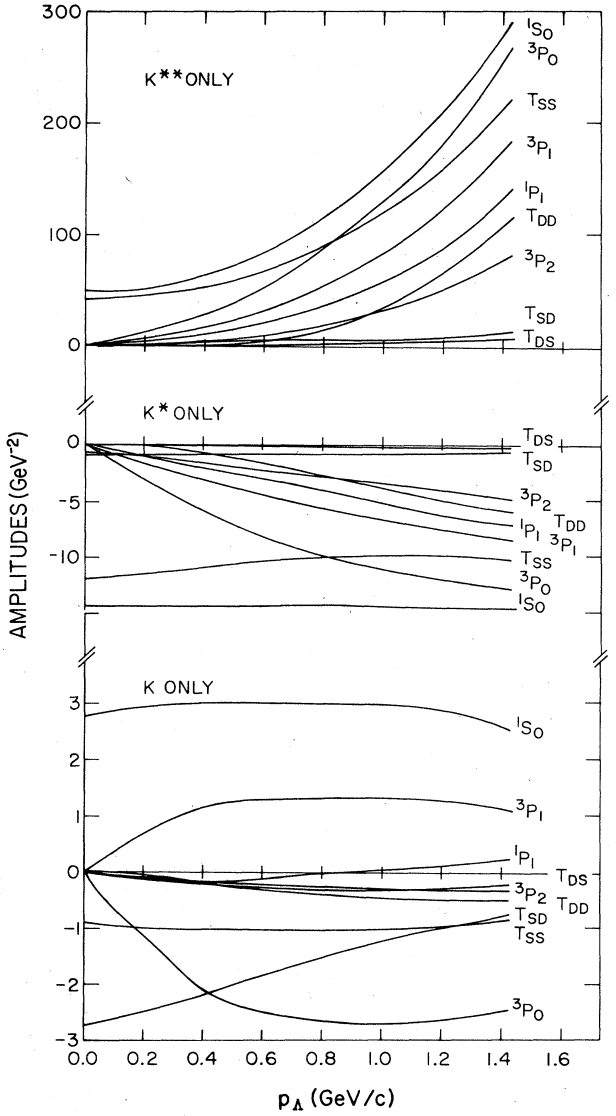

FIG. 9. The contribution of each meson to some of the partial-wave-projected amplitudes of Eq. (15). Initial and final state interactions are turned off. The results are expressed in the L-S basis, as a function of a laboratory momentum. Note that the K meson contributions are ordered as would be expected from a tensor force, while the K* and K** contributions are ordered in the sequence of an $L\cdot S$ force. Also note that the K* and K** are of opposite sign, and hence interfere destructively.

initial and final state interactions in Eq. (39); it is seen that for the energies studied in this paper the initial state interaction can make between a factor of 2 and a factor of 10 difference in cross section size. The final state interaction, which takes place between particles having considerably less relative speed, affects the size by a factor of about 1000. At present, there are few data other than those referenced here to constrain the outgoing $\bar{\Lambda}\Lambda$ final state interaction, about which almost nothing is known. Thus, our model will not be fully tested until *both* the initial and final state interactions are circumscribed by other, independent, reactions.

IV. A SIMPLE ONE-GLUON EXCHANGE MECHANISM

We turn our attention briefly to the possibility of describing the $\bar{p}p\to\bar{\Lambda}\Lambda$ reaction by means of a simple one-gluon exchange, as diagrammed in Fig. 1(b). In such a model the $\bar{q}\bar{q}$ and qq pairs present in the $\bar{p}$ and p ($\bar{u}\bar{d}$ and ud, respectively) act only as spectators. We use as the gluon propagator the form:[39]

$$-i\delta_{jk}[g^{\mu\nu}+(\zeta-1)p^{\mu}p^{\nu}/(p^2+i\epsilon)]/(p^2+i\epsilon)\ . \qquad (42)$$

Here ζ is a parameter responsible for fixing the appropriate gauge, while δ_{jk} is a Kronecker delta that operates in color space. Except for the appearance of the latter quantity, Eq. (42) is identical to the photon propagator. It is then used in a calculation paralleling those outlined in Sec. II C above to obtain the transition matrix T, from which we may calculate the usual observables. The form of Eq. (42) indicates that the result of calculating the polarization $\mathrm{Tr}(T\sigma T^{\dagger})$ will be identically zero. This result is contrary to experiments[38] done at incident momentum of 6 GeV/c. While a model based on Eq. (42) is most appropriate for the very high energy regime, it indicates the necessity for much more detailed quantum chromodynamics (QCD) calculations at the energies under discussion here.

Of course, large polarizations could be generated using initial and final state interactions, as was done above for the K-exchange model. It would, however, be much more interesting to be able to obtain them from a mechanism that involved quarks directly. Further work on this idea is in progress.

V. SUMMARY AND CONCLUSIONS

In the work described above, we have calculated the $\bar{p}p\to\bar{\Lambda}\Lambda$ process as a sum of t-channel strangeness-changing kaon exchanges. The K, K*, and K** mesons thus accounted for the detailed dynamics of our problem, while largely phenomenological initial and final state interactions were used to mitigate the effects of the strict Born approximation. In this way, we were able to account quite well for the data that exists on this reaction, and to make predictions to compare with the forthcoming high precision data[2] from the LEAR facility. In our calculations, only the K** coupling constant and the final state $\bar{\Lambda}\Lambda$ interaction parameters were adjusted. While the $\bar{\Lambda}\Lambda$ interaction was found to be energy dependent, the K** coupling constant was fixed globally for all fits.

It is clear from our work that the K** exchange plays a dramatic role in this process all the way down to threshold. This may occur simply because the process intrinsically involves high-momentum transfers; in any case it is a clear indication of the importance of short-range effects, especially the spin dynamics, and perhaps quark degrees of freedom. It was found that a delicate conspiracy exists between the K* and K**, and that the predicted quantum mechanical destructive interference between them is necessary to obtain agreement with the data. It is also clear from the above that while K exchange plays only a very small role at high energies, it does remain important near threshold. The calculation of the polarization and

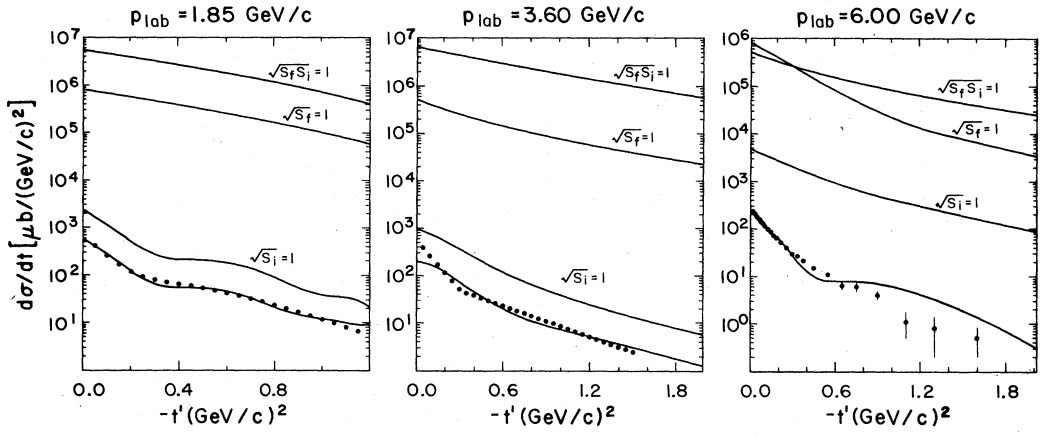

FIG. 10. The effects of the initial and final state interactions on the magnitude of the cross sections at 1.85, 3.6, and 6.0 GeV/c. The curves labeled $\sqrt{S_i}=1$ have no initial state interaction, the ones with $\sqrt{S_f}=1$ have no final state interaction, while the ones labeled $\sqrt{S_i S_f}=1$ have neither initial nor final state interactions. See Eq. (39). Due to the low momentum of the Λ's in the final state, neglect of their interaction has a large effect. See also Fig. 5.

spin correlation parameters is extremely sensitive to the detailed nature of the meson exchanges.

The initial and final state interactions were an important ingredient of our model, for they are responsible for generating the necessary large polarizations (via spin-orbit forces) and for damping the Born approximation cross section to the experimentally observed levels. In the absence of independent experimental information to constrain these interactions, the test of our meson exchange model was not as rigorous as it could have been. On the other hand, the available data may in fact now provide a useful piece of information about the K^{**} coupling constant, and the strength of the final state $\bar{\Lambda}\Lambda$ interaction. We eagerly await new data to test these ideas further.

Note added in proof: The polarization data of Atherton *et al.*[37] at 3.6 GeV/c was subsequently described by increasing the difference between μ_+ and μ_- for the $\bar{\Lambda}\Lambda$ interaction.

ACKNOWLEDGMENTS

This work was begun while R.A.E. was a sabbatical year visitor to the University of Pittsburgh and a faculty member at Carnegie-Mellon University. The generosity of the members of both of these institutions is greatly appreciated. During the course of the work we have benefited from discussion with several colleagues, including Bob Carlitz, Carl Carlson, V. Girija, Franz Gross, and Leonard Kisslinger. The members of LEAR experiment PS-185, especially Peter Barnes, Kurt Kilian, and Chris Maher, have shown continued interest in the work.

APPENDIX A: EMPIRICAL DETERMINATION OF THE POLARIZATIONS AND SPIN CORRELATIONS

We indicate below how to obtain several experimental observables from the basic amplitudes. We begin with a density matrix description of the initial uncorrelated beam and target, which we represent by a separable (outer) product:

$$\rho_{\bar{p}p}=\tfrac{1}{4}(1+\boldsymbol{\sigma}\cdot\mathbf{P})_{\bar{p}}(1+\boldsymbol{\sigma}\cdot\mathbf{P})_{p}\ .$$

After the interaction we have a density matrix describing the $\bar{\Lambda}\Lambda$ system:

$$\rho_{\bar{\Lambda}\Lambda}=T(\theta)\rho_{\bar{p}p}T(\theta)^{\dagger}\ ,$$

with $T(\theta)$ the strong interaction transition matrix [see Eq. (14)]. The matrix $\rho_{\bar{\Lambda}\Lambda}$ is not separable in general. However, as a 4×4 matrix it can be spanned by the basis set of 4×4 matrices $\sigma_\mu^{\bar{\Lambda}}\sigma_\nu^{\Lambda}$ obtained from outer products of the Pauli matrices $(\sigma_x,\sigma_y,\sigma_z)$ and the 2×2 unit matrix σ_0. We find

$$\rho_{\bar{\Lambda}\Lambda}=\tfrac{1}{4}I(\theta)\left[1_{\bar{\Lambda}}1_{\Lambda}+\boldsymbol{\sigma}\cdot\mathbf{P}^{\bar{\Lambda}}1_{\Lambda}+1_{\bar{\Lambda}}\boldsymbol{\sigma}\cdot\mathbf{P}^{\Lambda}+\sum_{kl}C_{kl}\sigma_k^{\bar{\Lambda}}\sigma_l^{\Lambda}\right],$$

$$=\tfrac{1}{4}I(\theta)C_{\mu\nu}\sigma_\mu^{\bar{\Lambda}}\sigma_\nu^{\Lambda}\ .$$

Here $(\mu,\nu=0,x,y,z)$ and $(k,l=x,y,z)$, while $C_{\mu0}=(1,P_x^{\bar{\Lambda}},P_y^{\bar{\Lambda}},P_z^{\bar{\Lambda}})$ and $C_{0\nu}=(1,P_x^{\Lambda},P_y^{\Lambda},P_z^{\Lambda})$. The quantities C_{kl} are the correlation coefficients C_{xx}, etc. The dynamics of the strong interaction is thus contained in the polarizations and spin correlation coefficients and the quality $I(\theta)$; i.e., the differential cross section.

We now wish to calculate ρ after *both* Λ particles undergo weak decay. Since each of these decays is independent, the weak decay transition matrix will be a product: $T^{w}_{\bar{\mu}\mu;\bar{m}m}=\bar{F}_{\bar{\mu}\bar{m}}F_{\mu m}$. The transition matrices F for the individual decays of $\bar{\Lambda}$ and Λ will differ by a phase due to charge conjugation. They can each be written as a product of a Wigner $\mathscr{D}$ function and a radial weak decay matrix element f_μ, e.g.,

$$F_{\mu m}=\left[\frac{2j+1}{4\pi}\right]^{1/2}\mathscr{D}^{j*}_{m\mu}(\phi,\theta,-\phi)f_\mu\ .$$

Here θ and ϕ refer to the outgoing proton in the rest frame of the Λ. For spin $\frac{1}{2}$ particles we have explicitly

$$F=\frac{1}{\sqrt{2\pi}}\begin{bmatrix} cf & s^*f \\ -sg & cg \end{bmatrix},$$

with $c=\cos\theta/2$ and $s=e^{i\phi}\sin\theta/2$. Quantities f and g represent the weak decay matrix elements $f_{+1/2}$ and $f_{-1/2}$, respectively. Using these definitions we find for the density matrix after both weak decays:

$$\rho_{\bar{p}p}=\tfrac{1}{4}I(\theta)C_{\mu\nu}(\bar{F}\sigma_\mu^{\bar{\Lambda}}\bar{F}^\dagger)(F\sigma_\nu^{\Lambda}F^\dagger) .$$

We use the convention that repeated indices are summed over. The matrices $(F\sigma_\mu F^\dagger)$ are

$$(F\sigma_0F^\dagger)=\frac{1}{2\pi}\begin{bmatrix}|f|^2 & 0\\ 0 & |g|^2\end{bmatrix},$$

$$(F\sigma_kF^\dagger)=\frac{1}{2\pi}\begin{bmatrix}|f|^2\cos\theta_k & a_k\\ a_k^* & -|g|^2\cos\theta_k\end{bmatrix},$$

$$(k=x,y,z) .$$

These forms are found after identifying the direction cosines with respect to the x and y axes in the Λ particle rest frame: $\cos\theta_x=\sin\theta\cos\phi$ and $\cos\theta_y=\sin\theta\sin\phi$. The a_k values are various products of c, s, f, and g; their exact form is not important here since only the traces of the matrices enter into the final result. Thus we obtain for the double differential cross section

$$\frac{d^2\sigma}{d\Omega\, d\bar{\Omega}}=\frac{M}{(2\pi)^2}\left[1+\bar{\alpha}\sum_k P_k^{\bar{\Lambda}}\cos\bar{\theta}_k+\alpha\sum_k P_k^{\Lambda}\cos\theta_k+\alpha\bar{\alpha}\sum_{kl}C_{kl}\cos\bar{\theta}_k\cos\theta_l\right],$$

with $\alpha=(|f|^2-|g|^2)/(|f|^2+|g|^2)$ and $\bar{\alpha}$ the same quantity for $\bar{f}$ and $\bar{g}$. Here $M=(|f|^2+|g|^2)(|\bar{f}|^2+|\bar{g}|^2)$. The angular distribution is easily obtained from this expression.

The normalization of Eq. (7) is found, by integrating over both $\bar{p}$ and p solid angles, to be $(16\pi^2)^{-1}$. For the case of no initial polarization, the above expression reduces to Eq. (7) in the text. To obtain the angular distribution for just one of the decays, we integrate the above over the solid angle of the unobserved particle, and find, for example:

$$W(\theta)=\frac{1}{4\pi}(1+\alpha P\cos\theta_y) .$$

From this we calculate the expectation value of $\cos\theta$: $\langle\cos\theta\rangle=\alpha P/3$. We thus obtain an expression for the polarization in terms of n experimentally measured quantities: $P=(3/\alpha n)\sum_{i=1}^n\cos\theta_i$. Using the same method to calculate the average of the product $\cos\bar{\theta}_k\cos\theta_l$ we find for the correlation coefficients C_{kl}:

$$C_{kl}=\frac{9}{\bar{\alpha}\alpha}\langle\cos\bar{\theta}_k\cos\theta_l\rangle=\frac{9}{\bar{\alpha}\alpha n}\sum_{i=1}^n(\cos\bar{\theta}_k\cos\theta_l)_i .$$

In the above cases, when no initial polarization is present, the "experimental" values of $\cos\theta$ are all measured with respect to the normal to the reaction plane in the rest frame of the particle. In order to find these quantities from the decay angles measured in the laboratory, a Lorentz transformation must be performed.

APPENDIX B: CREATION OPERATOR FORMULATION OF THE $\bar{N}N$ STATES

In this appendix we present the $\bar{N}N$ states using the language of creation and annihilation operators for the case of helicity states defined according to the phase conventions of Jacob and Wick.[5] The symmetry properties of parity, charge conjugation, and G parity are described and invoked to obtain the form of the amplitude given in Eq. (11). The relation between the helicity states of total angular momentum J and the states in the L-S coupling representation is displayed; each has its own particular usefulness.

The single particle plane-wave helicity states

The helicity state $|\mathbf{p},\lambda\rangle$ is obtained by rotating the state $|p\hat{\mathbf{z}},\lambda\rangle$ defined along the fixed $\hat{\mathbf{z}}$ axis into the direction $\hat{\mathbf{p}}$. In terms of the corresponding creation operators, we have

$$b_{\mathbf{p}\lambda}^\dagger=\sum_{m_s}\mathscr{D}^{1/2}_{m_s\lambda}(\hat{\mathbf{p}})b_{\mathbf{p}m_s}^\dagger$$

and (B1)

$$d_{\mathbf{p}\lambda}^\dagger=\sum_{m_s}\mathscr{D}^{1/2}_{m_s\lambda}(\hat{\mathbf{p}})d_{\mathbf{p}m_s}^\dagger$$

for nucleon and antinucleon creation, respectively. Thus we have

$$b_{\mathbf{p}\lambda}^\dagger|0\rangle=|\mathbf{p},\lambda\rangle=\sum_{m_s}\langle m_s|R(\hat{\mathbf{p}})|\lambda\rangle|\mathbf{p}m_s\rangle=R(\hat{\mathbf{p}})|p\hat{\mathbf{z}}\lambda\rangle .$$

Clearly, the above forms (and those for $b_{\mathbf{p}\lambda}$ and $d_{\mathbf{p}\lambda}$) preserve the usual anticommutation relations for such operators. Indeed, this canonical transformation permits us to describe the nucleon field operator in either a $\mathbf{p}m_s$ or $\mathbf{p}\lambda$ (helicity) basis as

$$\psi(x)=\sum_{m_s}\int\frac{d^3p}{(2\pi)^{3/2}}(\sqrt{m/E})[u(\mathbf{p},m_s)b_{\mathbf{p}m_s}e^{-ipx}+v(\mathbf{p},m_s)d_{\mathbf{p}m_s}^\dagger e^{ipx}] ,$$

$$=\sum_{\lambda}\int\frac{d^3p}{(2\pi)^{3/2}}(\sqrt{m/E})[u(\mathbf{p},\lambda)b_{\mathbf{p}\lambda}e^{-ipx}+v(\mathbf{p},\lambda)d_{\mathbf{p}\lambda}^\dagger e^{ipx}] ,$$

where $px = p_0 x_0 - \mathbf{p}\cdot\mathbf{x}$ and

$$u(\mathbf{p},\lambda) = \sum_{m_s} \mathscr{D}^{1/2}_{m_s\lambda}(\hat{\mathbf{p}}) u(\mathbf{p},m_s) = N \begin{pmatrix} 1 \\ \frac{\lambda p}{\omega} \end{pmatrix} \mathscr{D}_{+\lambda}(\hat{\mathbf{p}}) ,$$

$$v(\mathbf{p},\lambda) = \sum_{m_s} \mathscr{D}^{1/2}_{m_s\lambda}(\hat{\mathbf{p}}) v(\mathbf{p},m_s) = N \begin{pmatrix} \frac{-\lambda p}{\omega} \\ 1 \end{pmatrix} \mathscr{D}_{-\lambda}(\hat{\mathbf{p}}) \eta_\lambda .$$

In the above, we identify the particle and antiparticle spinors

$$u(\mathbf{p},m_s) = N \begin{pmatrix} 1 \\ \frac{\boldsymbol{\sigma}\cdot\mathbf{p}}{\omega} \end{pmatrix} \chi_{m_s}$$

and

$$v(\mathbf{p},m_s) = N \begin{pmatrix} \frac{\boldsymbol{\sigma}\cdot\mathbf{p}}{\omega} \\ 1 \end{pmatrix} \chi_{-m_s} \eta_{m_s} ,$$

where $\omega = \epsilon + m$, $N = [(\epsilon+m)/2m]^{1/2}$, and $\eta_\lambda = (-1)^{1/2-\lambda/2}$. From these the above helicity spinors follow. It is important to note for our later derivation that the operators $b^\dagger_{\mathbf{p}\lambda}$ and $d^\dagger_{\mathbf{p}\lambda}$ have a significant spinor property due to the appearance of the Wigner $\mathscr{D}$ function $\mathscr{D}^{1/2}(\hat{\mathbf{p}})$. That spinor property is

$$b^\dagger_{-\mathbf{p}\lambda} \mid_{-\mathbf{p}} = -b^\dagger_{+\mathbf{p}\lambda}$$

and

$$d^\dagger_{-\mathbf{p}\lambda} \mid_{-\mathbf{p}} = -d^\dagger_{+\mathbf{p}\lambda} ,$$

where we have $b^\dagger_{\mathbf{p}\lambda} \mid_{-\mathbf{p}} = b^\dagger_{-\mathbf{p}\lambda}$ and $d^\dagger_{\mathbf{p}\lambda} \mid_{-\mathbf{p}} = d^\dagger_{-\mathbf{p}\lambda}$, etc. The above minus sign arises from the $(-1)^{2j}$ factor contained in the $\mathscr{D}^j(\hat{\mathbf{p}})$ under two reversals $\mathbf{p} \to -\mathbf{p} \to +\mathbf{p}$. In contrast, the quantity $b^\dagger_{-\mathbf{p}m_s}$ evaluated at $\mathbf{p} \to -\mathbf{p}$ gives simply $b^\dagger_{-\mathbf{p}m_s} \mid_{-\mathbf{p}} = +b^\dagger_{\mathbf{p}m_s}$, etc. This spinor property and the phase factors η_λ permit us to recover all of the Jacob and Wick results using the creation operator formalism.

The $\bar{N}N$ states

Having defined the helicity creation operators for N and $\bar{N}$ we now describe the product states for the $\bar{N}N$ system. These plane-wave helicity states in the center-of-momentum frame, including the Jacob-Wick phases,[5] are defined by

$$\mid \mathbf{p}\lambda_1\lambda_2\rangle = \eta_{\lambda_2} d^\dagger_{\mathbf{p}\lambda_1} b^\dagger_{-\mathbf{p}\lambda_2} \mid 0\rangle, \quad \eta_\lambda = (-)^{1/2-\lambda/2} .$$

Here we take $\mathbf{p}_1 = -\mathbf{p}_2 = \mathbf{p}$. The individual helicity states are defined to satisfy

$$(\boldsymbol{\sigma}\cdot\mathbf{p}_1)_{\text{oper}} \mid \mathbf{p}_1\lambda_1\rangle = \lambda_1 p_1 \mid \mathbf{p}_1\lambda_1\rangle ,$$

and therefore

$$[\tfrac{1}{2}(\boldsymbol{\sigma}_1+\boldsymbol{\sigma}_2)\cdot\mathbf{p}]_{\text{oper}} \mid \mathbf{p}\lambda_1\lambda_2\rangle = \tfrac{1}{2}p(\lambda_1-\lambda_2) \mid \mathbf{p}\lambda_1\lambda_2\rangle .$$

The $\bar{N}N$ states are consequently eigenstates of the total helicity operator $(\mathbf{S}\cdot\mathbf{p})/\mid\mathbf{p}\mid$ with eigenvalue $(\lambda_1-\lambda_2)/2$.

The parity property of the above states is deduced from the parity properties of the individual $\bar{N}$ and N operators, which are

$$\mathscr{P} b^\dagger_{\mathbf{p}m_s} \mathscr{P}^\dagger = \eta_N b^\dagger_{-\mathbf{p}m_s}; \quad \mathscr{P} b^\dagger_{\mathbf{p}\lambda} \mathscr{P}^\dagger = \eta_N \eta_{-\lambda} b^\dagger_{-\mathbf{p}-\lambda}$$

and

$$\mathscr{P} d^\dagger_{\mathbf{p}m_s} \mathscr{P}^\dagger = \eta_N d^\dagger_{-\mathbf{p}m_s}; \quad \mathscr{P} d^\dagger_{\mathbf{p}\lambda} \mathscr{P}^\dagger = \eta_N \eta_{-\lambda} d^\dagger_{-\mathbf{p}-\lambda} .$$

Here $\eta_N = -\eta_{\bar{N}} = +1$ are the nucleon and antinucleon intrinsic parities. Using these relations leads to the result

$$\mathscr{P} \mid \mathbf{p}\lambda_1\lambda_2\rangle = \eta_N \eta_{\bar{N}} \eta_{\lambda_1} \eta_{-\lambda_2} \mid -\mathbf{p}-\lambda_1-\lambda_2\rangle$$

for plane-wave $\bar{N}N$ helicity states.

To study the operation of $\mathscr{P}$ on eigenstates of total angular momentum in the helicity basis, we first form these states by using the projection operator $\mathscr{D}^{*J}_{m\Lambda}(\hat{\mathbf{p}})$ on $\mid \mathbf{p}\lambda_1\lambda_2\rangle$. We have, with $N_J = [(2J+1)/4\pi]^{1/2}$

$$\mid pJM\lambda_1\lambda_2\rangle = N_J \int \mathscr{D}^{J*}_{m\Lambda}(\hat{\mathbf{p}}) d\hat{\mathbf{p}} \mid \mathbf{p}\lambda_1\lambda_2\rangle ;$$

a direct application of $\mathscr{P}$ to this state yields

$$\mathscr{P} \mid pJM\lambda_1\lambda_2\rangle = \eta_N \eta_{\bar{N}} (-1)^{s_1+s_2-J} \mid pJM-\lambda_1-\lambda_2\rangle ,$$

where one needs to use the spinor property of the $b^\dagger$ and $d^\dagger$ operators. This result shows that the state $\mid pJM\lambda_1\lambda_2\rangle$ is not an eigenstate of parity. Eigenstates of good JM and parity can easily be formed. One way to write such states is to use

$$\mid \pm\rangle_{JM} = \mid pJM\lambda_1\lambda_2\rangle \pm \eta_N \eta_{\bar{N}} (-1)^{J-s_1-s_2} \mid pJM-\lambda_1-\lambda_2\rangle$$

and thus obtain $\mathscr{P} \mid \pm\rangle_{JM} = \pm \mid \pm\rangle_{JM}$. The eigenstates of parity used in this work are given in Eq. (9); they are simply related to the above choice.

When examining the physical content of our results, especially near threshold, it is helpful to link the helicity basis states to the L-S coupling scheme. We do this by writing the state $\mid pJM\lambda_1\lambda_2\rangle$ in terms of the creation operators $b^\dagger$ and $d^\dagger$ for helicity states, and then using Eq. (B1) to expand them:

$$\mid pJM\lambda_1\lambda_2\rangle = N_J \int \mathscr{D}^{J*}_{M\Lambda}(\hat{\mathbf{p}}) d\hat{\mathbf{p}}\, \eta_{\lambda_2} d^\dagger_{\mathbf{p}\lambda_1} b^\dagger_{-\mathbf{p}\lambda_2} \mid 0\rangle ,$$

$$= N_J \sum_{M_s M_s'} \int \mathscr{D}^{J*}_{M\Lambda}(\hat{\mathbf{p}}) d\hat{\mathbf{p}}\, \eta_{\lambda_2} \mathscr{D}^{1/2}_{M_s\lambda_1}(\hat{\mathbf{p}}) \mathscr{D}^{1/2}_{M_s'\lambda_2}(-\hat{\mathbf{p}}) d^\dagger_{\mathbf{p}M_s} b^\dagger_{-\mathbf{p}M_s'} \mid 0\rangle .$$

By comparison, the L-S basis state $|pJMLS\rangle$ is

$$|pJMLS\rangle = N_J \sum \langle JM \,|\, LSM_L M_s\rangle \langle SM_s \,|\, \tfrac{1}{2}\tfrac{1}{2} M_s M_s'\rangle \int \mathscr{D}^{L*}_{M_L 0}(\hat{\mathbf{p}}) d\hat{\mathbf{p}}\, d^\dagger_{\mathbf{p}M_s} b^\dagger_{-\mathbf{p}M_s'} |0\rangle ,$$

$$= \sum \langle JM \,|\, LSM_L M_s\rangle \int Y^*_{LM_L}(\hat{\mathbf{p}}) d\hat{\mathbf{p}} (d^\dagger_{\mathbf{p}} \times b^\dagger_{-\mathbf{p}})_{SM_s} |0\rangle .$$

Rather straightforward manipulation of these forms gives the final standard result:

$$|pJM\lambda_1\lambda_2\rangle = \sum_{LS} C^J(\lambda_1\lambda_2 \,|\, LS)\, |pLSJM\rangle ,$$

with

$$C^J(\lambda_1\lambda_2 \,|\, LS) = \langle \tfrac{1}{2}\tfrac{1}{2}\lambda_1 - \lambda_2 \,|\, S\Lambda\rangle \langle LS0\Lambda \,|\, J\Lambda\rangle \times \left[\frac{2L+1}{2J+1}\right]^{1/2} .$$

Evaluation of the above coefficient leads to Eq. (13) given in the text. The connection between helicity states and LS states for a few cases of interest to our problem are given in Table V.

We turn now to the last of the symmetries needed for our problem: G parity. The operator for G parity consists of charge conjugation (C) followed by a rotation by π in isospin space about the isospin y-component axis. G parity is conserved in strong interactions. Thus, $G = e^{i\pi\tau_y} C$. In the conventions used below, C operating on the physical nucleon states gives $C\,|\,\mathrm{p}\rangle = |\,\bar{\mathrm{p}}\rangle$ and $C\,|\,\mathrm{n}\rangle = |\,\bar{\mathrm{n}}\rangle$. However, the operators $b^\dagger_{\mathbf{p}\lambda m_\tau}$ and $d_{\mathbf{p}\lambda m_\tau}$ create states of good isospin T and projection m_τ: $b^\dagger_{\mathbf{p}\lambda m_\tau}|0\rangle = |N\mathbf{p}\lambda m_\tau\rangle$ and $d^\dagger_{\mathbf{p}\lambda m_\tau}|0\rangle = |\bar{N}\mathbf{p}\lambda m_\tau\rangle$. The relation of these states to the physical nucleon states is as follows:

$$|\,\mathrm{N}\mathbf{p}\lambda\tfrac{1}{2}\rangle = |\,\mathrm{p}\rangle, \quad |\,\mathrm{N}\mathbf{p}\lambda - \tfrac{1}{2}\rangle = |\,\mathrm{n}\rangle ,$$

$$|\,\bar{\mathrm{N}}\mathbf{p}\lambda\tfrac{1}{2}\rangle = -|\,\bar{\mathrm{n}}\rangle, \quad |\,\bar{\mathrm{N}}\mathbf{p}\lambda - \tfrac{1}{2}\rangle = |\,\bar{\mathrm{p}}\rangle .$$

Thus, the creation operators obey the following transformation rules:

$$\hat{\mathbf{C}} b^\dagger_{\mathbf{p}\lambda m_\tau} \hat{\mathbf{C}}^\dagger = (-)^{1/2-m_\tau} d^\dagger_{\mathbf{p}\lambda - m_\tau} ,$$

$$\hat{\mathbf{C}} d^\dagger_{\mathbf{p}\lambda m_\tau} \hat{\mathbf{C}}^\dagger = -(-)^{1/2-m_\tau} b^\dagger_{\mathbf{p}\lambda - m_\tau} .$$

Using this result it follows that the G-parity operator acts in the following way:

$$G\,|\,\mathrm{N}\mathbf{p}\lambda\tfrac{1}{2}m_\tau\rangle = |\,\bar{\mathrm{N}}\mathbf{p}\lambda\tfrac{1}{2}m_\tau\rangle,$$

$$G\,|\,\bar{\mathrm{N}}\mathbf{p}\lambda\tfrac{1}{2}m_\tau\rangle = -|\,\mathrm{N}\mathbf{p}\lambda\tfrac{1}{2}m_\tau\rangle, \qquad G^2 = -1 = (-)^{2I} .$$

To investigate the effect of G on the $\bar{\mathrm{N}}\mathrm{N}$ states, we first form a two-particle state of good isospin:

$$|\,\bar{\mathrm{N}}\mathrm{N}pJM\lambda_1\lambda_2 II_3\rangle = N_J \int \mathscr{D}^{J*}_{M\Lambda}(\hat{\mathbf{p}}) d\hat{\mathbf{p}}\, \eta_{\lambda_2} \times (d^\dagger_{\mathbf{p}\lambda_1} \times b^\dagger_{-\mathbf{p}\lambda_2})_{II_3} |0\rangle .$$

Application of C to this state yields

$$C\,|\,\bar{\mathrm{N}}\mathrm{N}pJM\lambda_1\lambda_2 II_3\rangle = (-)^{I+J}(-)^{I-I_3} \times |\,\bar{\mathrm{N}}\mathrm{N}pJM\lambda_2\lambda_1 I - I_3\rangle .$$

Note the interchange of helicity labels. On the other hand, the full G operator gives

$$G\,|\,\bar{\mathrm{N}}\mathrm{N}pJM\lambda_1\lambda_2 II_3\rangle = (-)^{I+J}\,|\,\bar{\mathrm{N}}\mathrm{N}pJM\lambda_2\lambda_1 II_3\rangle .$$

The G parity of the $|nJ\rangle$ basis set [Eq. (9)] is now easily determined to be $(-)^{J+I}$ for $n = 2,3,4$ and $-(-)^{J+I}$ for $n = 1$. Thus, if the T matrix is G-parity conserving, we find that $n = 2,3,4$ states may connect to each other, but not to $n = 1$. From the structure developed earlier, we see also that based on parity alone, states $n = 1$ and $n = 4$ could connect to each other but not to $n = 2,3$. These rules therefore account for the matrix form given in Eq. (11). Using the parity, time reversal, and G-parity properties of these helicity states, one can deduce directly Eq. (14).

This work was supported by the U.S. Department of Energy and the National Science Foundation.

[1] *Physics at LEAR with Low-Energy Cooled Antiprotons,* edited by U. Gastaldi and R. Klapisch (Plenum, New York, 1984).
[2] P. D. Barnes, P. Birien, B. Bonner, R. A. Eisenstein, W. Eyrich, J. Franz, A. Hofmann, T. Johansson, K. Kilian, S. Polikanov, E. Rossle, H. Schmitt, and W. Wharton, CERN Report CERN/PSCC/81-69, 1981.
[3] L. Durand and J. Sandweiss, Phys. Rev. **135**, B540 (1964).
[4] M. Perl, *High Energy Hadron Physics* (Wiley, New York, 1974).
[5] M. Jacob and G. C. Wick, Ann. Phys. (N.Y.) **7**, 404 (1959).
[6] N. J. Sopkovich, Ph.D. thesis, Carnegie-Mellon University, 1962; Nuovo Cimento **26**, 186 (1962).
[7] H. D. D. Watson, Nuovo Cimento **29**, 1338 (1963).
[8] H. Hogaasen and J. Hogaasen, Nuovo Cimento **40**, 560 (1965); **39**, 941 (1965).
[9] G. Cohen-Tannoudji and H. Navelet, Nuovo Cimento **37**, 1511 (1965).
[10] J. H. R. Migneron and H. D. D. Watson, Phys. Rev. **166**, 1654 (1968); H. D. D. Watson and J. H. R. Migneron, Phys. Lett. **19**, 424 (1965).
[11] L. Durand and Yam Tsi Chu, Phys. Rev. **137**, 1530 (1965).
[12] G. C. Summerfield, Nuovo Cimento **23**, 867 (1962).
[13] D. Bessis, C. Itzykson, and M. Jacob, Nuovo Cimento **27**, 376 (1963).

[14]S. M. Berman and R. J. Oakes, Nuovo Cimento **29**, 1329 (1963).
[15]C. H. Chan, Phys. Rev. **133**, B431 (1964).
[16]E. Eisenhandler, W. R. Gibson, C. Hojvat, P. I. P. Kalmes, L. C. Y. Lee, T. W. Pritchard, E. C. Usher, D. T. Williams, M. Harrison, W. H. Range, M. A. R. Kemp. A. D. Rush, J. N. Woulds, G. T. J. Arnison, A. Astbury, D. P. Jones, and A. S. L. Parsons, Nucl. Phys. **B113**, 1 (1976).
[17]C. Daum, F. C. Erne, J. P. Lagnaux, J. C. Sens, M. Steuer, and F. Udo, Nucl. Phys. **B6**, 617 (1968).
[18]A. Sundaram and K. Srinivasa Rao, Nuovo Cimento **61A**, 755 (1969).
[19]B. Sadoulet, Nucl. Phys. **B53**, 135 (1973).
[20]F. J. Hadjioannou and P. N. Poulopoulos, Lett. Nuovo Cimento **3**, 384 (1970).
[21]M. Saleem and M. Ali, Lett. Nuovo Cimento **32**, 425 (1981).
[22]G. Plaut, Nucl. Phys. **B35**, 221 (1971).
[23]Discussed in, P. Handler, R. Grobel, L. Pondrom, M. Sheoff, C. Wilkinson, P. T. Cox, J. Dworkin, O. E. Overseth, K. Heller, T. Devlin, L. Deck, K. B. Luk, R. Rameika, P. Skubic, and G. Bunce, Phys. Rev. D **25**, 639 (1982).
[24]M. M Nagels, Th. A. Rijken, J. J. DeSwart, G. C. Oades, J. L. Petersen, A. C. Irving, C. Jarlskog, W. Pfeil, H. Pilkuhn, and H. P. Jakob, Nucl. Phys. **B147**, 189 (1979); M. M. Nagels, T. A. Rijken, and J. J. de Swart, Phys. Rev. D **15**, 2547 (1977); **20**, 1633 (1979).
[25]A. Rosenthal, private communication.
[26]J. D. Bjorken and S. Drell, *Relativistic Quantum Mechanics* (McGraw-Hill, New York, 1964).
[27]D. M. Brink and G. R. Satchler, *Angular Momentum,* 2nd ed. (Clarendon, Oxford, 1968).
[28]K. Gottfried and J. D. Jackson, Nuovo Cimento **34**, 735 (1964).
[29]M. H. Ross and G. L. Shaw, Phys. Rev. Lett. **12**, 627 (1964).
[30]P. K. Williams, Phys. Rev. **181**, 1963 (1969).
[31]Milton Abramowitz and Irene A. Stegun, *Handbook of Mathematical Functions* (Dover, New York, 1964).
[32]H. Pilkuhn, *Relativistic Particle Physics* (Springer, Berlin, 1979); *The Interaction of Hadrons* (North-Holland, Amsterdam, 1967).
[33]P. R. Auvil and J. J. Brehm, Phys. Rev. **145**, 1152 (1966).
[34]J. Bystricky, F. Lehar, and P. Winternitz, J. Phys. (Paris) **39**, 1 (1978); N. Hoshizaki, Prog. Theor. Phys., Suppl. **42**, 107 (1968).
[35]V. Flaminio, W. G. Moorhead, D. R. O. Morrison, and N. Rivoire, CERN Report CERN-HERA-84-01, 1984.
[36]B. Jayet, M. Gailloud, Ph. Rosselet, V. Vuillemin, S. Vallet, M. Bogdanski, E. Jeannet, C. J. Campbell, J. Dawber, and D. N. Edwards, Nuovo Cimento **45A**, 371 (1978).
[37]H. W. Atherton, B. R. French, J. P. Moebes, and E. Quercigh, Nucl. Phys. **B69**, 1 (1974).
[38]H. Becker, G. Blanar, W. Blum, V. Chabaud, J. DeGroot, H. Dietl, J. Gallivan, W. Kern, E. Lorenz, G. Lutjens, G. Lutz, W. Manner, R. Mount, D. Notz, R. Richter, U. Stierlin, and M. Turala, Nucl. Phys. **B141**, 48 (1978).
[39]C. Quigg, *Gauge Theories of the Strong, Weak, and Electromagnetic Interactions* (Benjamin, Reading, Mass., 1983).